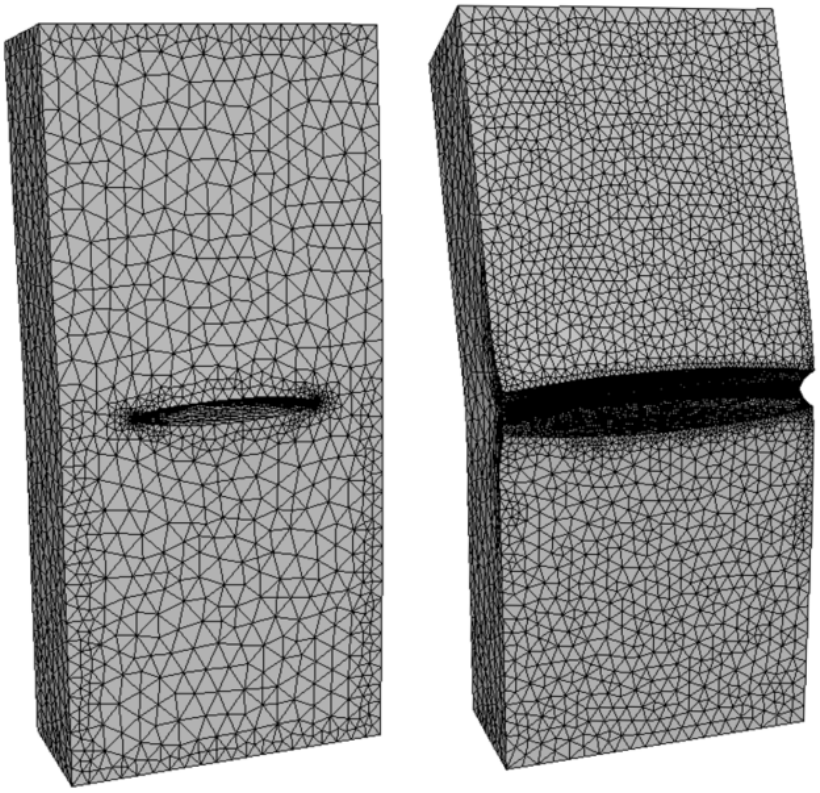

# Potentials and limitations in finite element based crack propagation analysis using FRANC3D

Master's thesis in Applied Mechanics

FILIP ELFVING
JONAS HÆG

Department of Mechanics and Maritime Sciences

CHALMERS UNIVERSITY OF TECHNOLOGY
Gothenburg, Sweden 2020
www.chalmers.se

Master's thesis in Applied Mechanics

# Potentials and limitations in finite element based crack propagation analysis using FRANC3D

FILIP ELFVING
JONAS HÆG


CHALMERS
UNIVERSITY OF TECHNOLOGY

Department of Mechanics and Maritime Science
*Division of Dynamics*
Chalmers University of Technology
Gothenburg, Sweden 2020

Potentials and limitations in finite element based crack propagation analysis using FRANC3D
Filip Elfving
Jonas Hæg



Supervisor: Tomas Månsson and Sushovan Roychowdhury, GKN Aerospace Sweden
Examiner: Anders Ekberg, Department of Mechanics and Maritime Science

Master's Thesis 2020:26
Department of Mechanics and Maritime Science
Division of Dynamics
Chalmers University of Technology
SE-412 96 Gothenburg
Telephone +46 31 772 1000

Cover: Finite element model of a cracked specimen illustrating two different crack sizes during a crack propagation analysis.

Typeset in LaTeX
Printed by Chalmers Reproservice
Gothenburg, Sweden 2020

Potentials and limitations in finite element based crack propagation analysis using FRANC3D
Master's thesis in Applied Mechanics
FILIP ELFVING, JONAS HÆG
Department of Mechanics and Maritime Sciences
Division of Dynamics
Chalmers University of Technology

# Abstract

About 80% to 95% of all structural failures occur due to a fatigue mechanism[1]. Accurate fatigue assessment is therefore of great importance. This thesis focuses on a finite element analysis based approach, implemented in the program FRANC3D, to simulate crack propagation under fatigue loading. This approach is not commonly used at GKN, where the thesis was carried out. FRANC3D offers the users many options, the effect of which has not been previously investigated at GKN. In this thesis, a sensitivity study of various settings in FRANC3D was performed for propagation analyses of a semi-elliptical surface crack in a rectangular test specimen. A group of settings were identified to be recommended and were later used for fatigue assessment of Kb test specimens for two different load types: tensile and four-point bending. The results were validated against handbook-type solutions, provided by NASGRO, and towards test results. Fatigue crack growth assessment was also performed for an embedded crack in a circular specimen—a load case not supported within NASGRO. A statistical evaluation of the finite element based approach gave similar results as the handbook-type solutions and matched the test results with respect to mean fatigue life. Thus, this thesis can be considered to have validated FRANC3D for GKN's internal use. This opens up the opportunity for more accurate fatigue life calculations for components with complex geometry and complex thermal and mechanical loading histories.

Keywords: Fatigue, crack propagation, FRANC3D, NASGRO, fracture mechanics, SIF, $M$-integral, surface crack, embedded crack.

[1] "How to predict fatigue life", *DESIGN NEWS*, Dec. 2001, [Online]. Available: `https://www.designnews.com/materials-assembly/how-predict-fatigue-life/33271708340745`, Accessed on: May 27, 2020.

# Acknowledgements

We would like to express our very great appreciation to Dr. Tomas Månsson and Dr. Sushovan Roychowdhury, our supervisors at GKN Aerospace Engine Systems, for their valuable and constructive guidance during the planning and development of this Master's thesis work. We would also like to thank Dr. Thomas Hansson and Jonas Kullgren for supporting us with valuable information about the testing procedure and also allowing us to visit the fatigue testing facility. Furthermore, we would like to thank our examiner Prof. Anders Ekberg who has earned our gratitude for contributing with his external views on the thesis report, and also support in finding relevant literature. Finally, huge thanks to our family an all colleagues at the Global Technology Centre at GKN for great help and support during the entire thesis work.

Filip Elfving, Jonas Hæg, Gothenburg, June 2020

# Nomenclature

## Abbreviations

| | |
|---|---|
| ASCII | American Standard Code for Information Interchange |
| B.C. | Boundary condition |
| FAC | Fracture Analysis Consultants |
| FE | Finite Element |
| FEA | Finite Element Analysis |
| BEM | Boundary Element Method |
| GKN | Guest, Keen & Nettlefolds |
| GUI | Graphical User Interface |
| LEFM | Linear Elastic Fracture Mechanics |
| NASA | National Aeronautics and Space Administration |
| RBM | Rigid Body Motion |
| GTC | Global Technology Centre |
| SIF | Stress Intensity Factor |
| SwRI | Southwest Research Institute |

## List of symbols

| | | |
|---|---|---|
| $a$ | Crack length | mm |
| $a_{\text{end}}$ | End crack length | mm |
| $a_{\text{start}}$ | Start crack length | mm |
| $c$ | Half crack width | mm |
| $\overline{c}_{\text{start}}$ | Median start crack width (half) | mm |
| $e$ | Error in prediction | - |
| $E$ | Young's modulus | MPa |
| $F$ | Force | N |
| $h$ | Height | mm |
| $J$ | Value of J integral | $\text{J/mm}^2$ |
| $K$ | SIF | $\text{MPa}\sqrt{\text{mm}}$ |
| $K_{\text{c}}$ | Fracture toughness | $\text{MPa}\sqrt{\text{mm}}$ |
| $K_{\text{max}}$ | Maximum SIF during cycle | $\text{MPa}\sqrt{\text{mm}}$ |
| $K_{\text{min}}$ | Minimum SIF during cycle | $\text{MPa}\sqrt{\text{mm}}$ |
| $\Delta K_{\text{th}}$ | Threshold SIF range | $\text{MPa}\sqrt{\text{mm}}$ |
| $m$ | Number of Gaussian integration points | - |
| $M$ | Value of M integral | $\text{J/mm}^2$ |
| $N$ | Number of cycles | Cycles |
| $N_{\text{pred.}}$ | Predicted number of cycles | Cycles |
| $N_{\text{test}}$ | Number of cycles from test | Cycles |
| $N_{\text{tran.}}$ | Number of cycles until transition | Cycles |
| $R$ | Stress ratio | - |

| | | |
|---|---|---|
| $S_{\max}$ | Maximum nominal stress | MPa |
| $S_{\min}$ | Minimum nominal stress | MPa |
| $t$ | Thickness | mm |
| $T$ | Temperature | °C |
| $u$ | Displacement | mm |
| $V^*$ | Volume of tube shaped integration domain | $mm^3$ |
| $w$ | Width | mm |
| $w_p$ | Weights used for Gaussian quadrature | - |
| $W$ | Strain energy density | $J/mm^3$ |
| | | |
| $\beta$ | SIF reduction factor for growth at surface | - |
| $\theta$ | Angle | ° |
| $\epsilon$ | Strain | - |
| $\nu$ | Poisson's ratio | - |
| $\sigma_y$ | Yield stress | MPa |
| $\tau$ | Shear stress | MPa |

# List of Figures

# List of Tables

# 1

# Introduction

There is a large interest in developing lightweight aerospace components today due to increase energy efficiency demands, which leads to demands on reduced fuel consumption. The main driving force is likely to reduce the carbon footprint, but other benefits are also obtained from lightweight design, these include improved flight performance and reduced operating costs for airlines [1].

One aspect of lightweight design is to select appropriate materials. The selection of structural materials and designs in the aerospace industry is based on several requirements, i.e. mechanical, physical and chemical properties [1]. The fatigue durability is one of these properties that is affected by the lightweight design. It is therefore of interest to find more accurate methods for performing crack propagation analyses and predicting the fatigue life.

## 1.1 Background

There are several codes available for crack propagation analyses. The codes considered in this thesis work are based on two different approaches to crack propagation analyses.

The first approach is the one used at GKN today, it is based on handbook-type solutions. This approach is implemented in NASGRO, developed jointly by SwRI and NASA, NASGRO is widely used in industry today [2] and includes many applications for aircraft and spacecraft components. The SIFs are calculated from tabulated values or analytical expressions to conjugate to the stresses in the crack plane. These tabulated values are based on specific crack cases, e.g. a surface crack in a cylinder or an embedded crack in a plate. For more complex geometries, it is possible to evaluate the stresses at the crack plane for an uncracked model with FEM, and import these into NASGRO.

The second approach is a numerical approach based on FEM that is included in FE-codes such as ANSYS or ABAQUS which have builtin solvers for crack propagation analyses.

The main difference between the two approaches is that the SIF solutions in the

first approach are calculated for a limited number of various crack types, geometries and loading. In the second approach, the obtained stress field from the FE-analysis is used to calculate the SIFs. This is possible in NASGRO as well, but only for stresses from an uncracked model. Hence NASGRO is not taking into account, e.g. the stress variation along the crack front. Including FE as an integrated tool makes it possible to calculate SIFs needed to perform crack propagation analyses for more non-standard components where handbook-type solutions are not available.

This thesis focuses on the FE-based approach, and in particular the implementation in the code FRANC3D that can use ANSYS as FE-solver in conjunction with a crack propagation evaluation and mesh-updating routine. FRANC3D uses the calculated stress field for the cracked FE-model and evaluates the SIFs, e.g. by use of the $M$-integral method. The predicted updated crack front is then used as input for a new mesh generated by FRANC3D. The problem is solved repeatedly in this manner.

The difference between predictions using the two approaches needs to be investigated more in detail. Knowledge about how FRANC3D predicts the new crack front and performs the re-meshing around the crack front are also parts that have to be explored.

## 1.2 Purpose

The main purpose of this thesis work is to evaluate the FE-based crack propagation program FRANC3D in comparison to handbook-type solutions and experiments. Effects of different crack propagation prediction model parameters within FRANC3D will be studied along with mesh sensitivity and accuracy of the simulations. A collection of suitable settings for crack propagation analysis will also be presented.

The main aim is reached through the following steps:

- Familiarise with the topic of fracture mechanics as applied to industrial problems and literature studies.
- Learn to use and compare the required programs: NASGRO[1], ANSYS[2] and FRANC3D[3] for a simplified test case.
- Create FE-models of fatigue test specimens in ANSYS. Apply appropriate boundary conditions, initial crack sizes, material properties etc.
- Investigate and select appropriate settings for crack propagation analysis in FRANC3D.
- Validate simulations against available test data based on, i.e. cycles to failure, cycles to a pre-determined crack size and crack shape.

[1]NASGRO, SwRI, version 9.1
[2]ANSYS Mechanical APDL, Ansys, Inc., version 19.1
[3]FRANC3D, FAC, Inc., version 7.4.2

- Perform crack propagation analyses in FRANC3D for a configuration not readily available in NASGRO. Apply suitable assumptions for the NASGRO calculations and compare results.

## 1.3 Scope and limitations

LEFM is assumed to be applicable and all analyses were performed for Mode I loading only. Crack propagation under thermal load was not considered, i.e no temperature difference was assumed. An explicit modelling of contact for the compressive part of fatigue cycle was excluded in the analyses.

Several codes have possibilities to perform crack propagation analyses, but this theses is limited to the following three programs: ANSYS, NASGRO and FRANC3D. The considered crack types were limited to two types: surface crack and embedded crack. The considered initial crack shapes were limited to semi-circular and semi-elliptical.

All required material and test data were provided by GKN for two different materials: denoted Material A and Material B. Material A is a nickel-chromium based alloy and Material B a titanium alloy.

# 2

# Theory

## 2.1 Fracture mechanics basics

A crack can experience three modes of loading as shown in Figure 2.1. Mode I loading is when the load is applied normal to the crack plane and is also called the opening mode. For Mode II the load acts as an in-plane shear load where the loading makes one crack face slide relative to the other. Mode III corresponds to out-of-plane shear loading [3, p. 52].

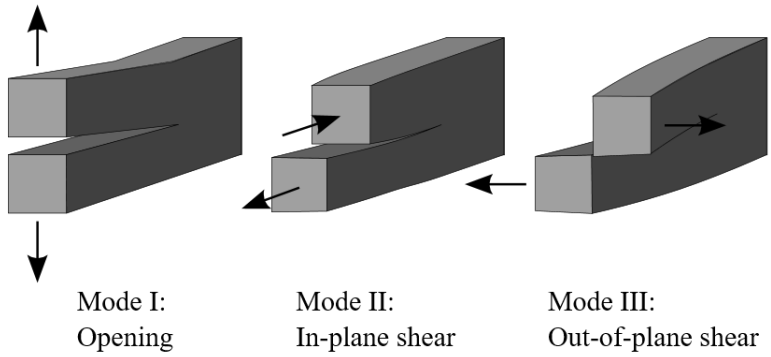


**Figure 2.1:** Fracture modes. Taken from [4]

From theory of fracture mechanics a useful quantity called the SIF, denoted as $K$, can be defined. The SIF is a measure of the severity of the crack loading as affected by crack size, the stress situation and the geometry of the considered configuration [5, p.339]. When defining $K$, assumptions are made that the material behaves in a linear-elastic manner. This approach is called LEFM and is valid if the plastic zone is sufficiently small as compared to the region influenced by the stress singularity at the crack tip, denoted the K-dominated stress field. In order to determine what is a sufficiently small plastic zone, Dowling [5, p. 388] presents an overall limit that defines when LEFM is applicable for plane strain condition under static loading, see Equation (2.1).

$$t,\ a,\ (b-a),\ h \geq 2.5\left(\frac{K}{\sigma_{\mathrm{y}}}\right)^2 \tag{2.1}$$

In Equation (2.1), $\sigma_{\mathrm{y}}$ is the yield stress, $t$ is the thickness, $a$ is the crack length, $b$ is the width of the specimen and $h$ is the height measured from the crack plane. A configuration with a defined crack and its plastic zone together with the larger K-field that must exist for LEFM to be valid is seen in Figure 2.2.

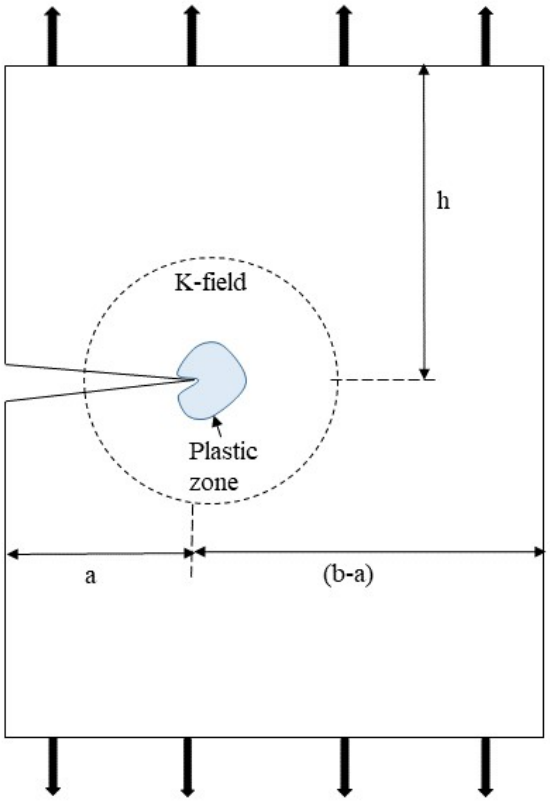


**Figure 2.2:** An illustration of a crack with its plastic zone and the required K-field for LEFM to be applicable

The stress and displacement fields close to the crack front can be estimated from the first terms in an asymptotic stress and displacement solution which is related to the SIFs, [6, p. 244-245]. The stress field is defined as

$$\begin{bmatrix}\sigma_x\\ \sigma_y\\ \tau_{xy}\\ \tau_{yz}\\ \tau_{zx}\end{bmatrix} = \frac{1}{\sqrt{2\pi r}}\begin{bmatrix}\cos\frac{\theta}{2}(1-\sin\frac{\theta}{2}\sin\frac{3\theta}{2}) & -\sin\frac{\theta}{2}(2+\cos\frac{\theta}{2}\cos\frac{3\theta}{2}) & 0\\ \cos\frac{\theta}{2}(1+\sin\frac{\theta}{2}\sin\frac{3\theta}{2}) & \sin\frac{\theta}{2}\cos\frac{\theta}{2}\cos\frac{3\theta}{2} & 0\\ \cos\frac{\theta}{2}\sin\frac{\theta}{2}\cos\frac{3\theta}{2} & \cos\frac{\theta}{2}(1-\sin\frac{\theta}{2}\sin\frac{3\theta}{2}) & 0\\ 0 & 0 & \cos\frac{\theta}{2}\\ 0 & 0 & -\sin\frac{\theta}{2}\end{bmatrix}\begin{bmatrix}K_{\mathrm{I}}\\ K_{\mathrm{II}}\\ K_{\mathrm{III}}\end{bmatrix} \tag{2.2}$$

An illustration of the local coordinate system at the crack front together with definitions describing the geometry of the crack, is shown in Figure 2.3. Here $\sigma_z = 0$ in all modes (I-III) for plane stress. For plane strain condition $\sigma_z = 0$ in Mode III, while in Mode I and II it becomes

$$\sigma_z = \nu(\sigma_x + \sigma_y). \tag{2.3}$$

The displacement field under plane strain conditions is approximately

$$\begin{bmatrix} u_x \\ u_y \\ u_z \end{bmatrix} = \frac{2(1+\nu)}{E}\sqrt{\frac{r}{2\pi}} \begin{bmatrix} \cos\frac{\theta}{2}(1-2\nu+\sin^2\frac{\theta}{2}) & \sin\frac{\theta}{2}(2-2\nu+\cos^2\frac{\theta}{2}) & 0 \\ \sin\frac{\theta}{2}(2-2\nu-\cos^2\frac{\theta}{2}) & \cos\frac{\theta}{2}(2\nu-1+\sin^2\frac{\theta}{2}) & 0 \\ 0 & 0 & 2\sin\frac{\theta}{2} \end{bmatrix} \begin{bmatrix} K_{\mathrm{I}} \\ K_{\mathrm{II}} \\ K_{\mathrm{III}} \end{bmatrix} \tag{2.4}$$

while in plane stress conditions, the displacement field can be found in textbooks, e.g. [6, p. 244-245].

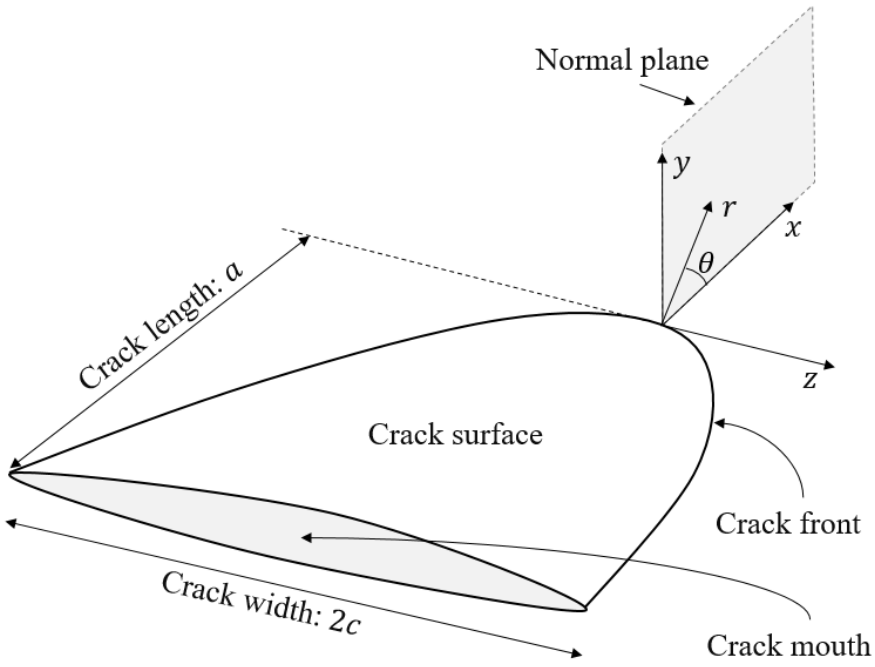


**Figure 2.3:** Local crack front coordinate system and crack geometry definitions

## 2.2 Methods for calculating SIFs

Stresses and displacements in the vicinity of the crack tip can be expressed according to Equation (2.2) and (2.4) regardless of loading and geometry of the specimen. One method to calculate the SIFs is to first solve for the displacement field using FEM and then employ the relationship in Equation (2.4) to solve for the $K$ values. This

method is called the displacement correlation method and has been shown to be less robust, than e.g. energy or integration methods [7], and therefore not so frequently used today.

In this thesis, handbook-type solutions and numerical methods, i.e. path independent integration methods, were considered. Two path independent integration methods, $J$- and $M$-integrals, will be explained more in detail in sections 2.2.2 and 2.2.3.

### 2.2.1 Handbook solutions

As formulated in the NASRGO manual [8, p.9], the SIFs can be expressed as follows

$$K = [S_0F_0 + S_1F_1 + S_2F_2 + S_3F3 + S_4F_4]\sqrt{\pi a} \tag{2.5}$$

where the stress quantities $S_0$ to $S_4$ correspond to different types of loading and how they are applied, e.g. $S_0$ and $S_1$ are the applied tension/compression and bending in thickness direction respectively. $F$ are geometric correction factors for each type of loading and are specifically derived for each crack case. More on handbook-type solutions can be found in various mechanical handbooks or in fatigue and fracture mechanics course literature, see [3, 5, 6].

### 2.2.2 $J$-integral

Considering an arbitrary path $\Gamma$ around the crack tip, the $J$-integral can be defined as

$$J = \int_\Gamma \left( W n_x - T_i \frac{\partial u_i}{\partial x} \right) ds \tag{2.6}$$

where $W = \frac{1}{2}\sigma_{ij}\epsilon_{ij}$ is the strain energy density, $n_i$ is the outpointing normal, $T_i = \sigma_{ij}n_j$ is the traction and $u_i$ are the displacements [3, p.126].

A relationship between the $J$-integral and the SIFs, in the context of LEFM [6, p.248], can be expressed as follows

$$G = J = \frac{K_{\mathrm{I}}^2}{E'} + \frac{K_{\mathrm{II}}^2}{E'} + \frac{(1+\nu)K_{\mathrm{III}}^2}{E} \tag{2.7}$$

where $G$ is the energy release rate, $\nu$ the Poisson's ratio and $E'$ is Young's modulus, see Equation (2.8).

$$E' = \begin{cases} E & \text{Plane stress} \\ \frac{E}{1-\nu^2} & \text{Plane strain} \end{cases} \tag{2.8}$$

### 2.2.3 $M$-integral

It has been shown that the $M$-integral can be developed from the $J$-integral as a way to evaluate the SIFs for all three fracture modes [9]. To formulate the $M$-integral, two

independent equilibrium states are assumed and superposed according to Equation (2.9). The actual state (with superscript (1)) is obtained from the FE-solution of the actual boundary value problem. The auxiliary state (with superscript (2)) is obtained from the known asymptotic stress and displacement fields (Equations (2.2) to (2.4)). This split is possible for a linear elastic material [10].

$$\begin{aligned} \sigma_{ij} &= \sigma_{ij}^{(1)} + \sigma_{ij}^{(2)} \\ \epsilon_{ij} &= \epsilon_{ij}^{(1)} + \epsilon_{ij}^{(2)} \\ u_i &= u_i^{(1)} + u_i^{(2)} \\ K_i &= K_i^{(1)} + K_i^{(2)} \end{aligned} \tag{2.9}$$

Substitution of the stress, strain and displacement fields (Equation (2.9)) into Equation (2.6) gives

$$J_1 = J_1^{(1)} + J_1^{(2)} + M_1^{(1,2)} \tag{2.10}$$

where the interaction term $M_1^{(1,2)}$ is called the $M$-integral. This term is defined as the first $M$-integral formulation denoted with subscript 1. $M_1^{(1,2)}$, $J_1^{(1)}$ and $J_1^{(2)}$ are expressed as follows:

$$\begin{aligned} J_1^{(1)} &= \int (W^{(1)} n_x - T_i^{(1)} \frac{\partial u_i^{(1)}}{x}) ds \\ J_1^{(2)} &= \int (W^{(2)} n_x - T_i^{(2)} \frac{\partial u_i^{(2)}}{x}) ds \\ M_1^{(1,2)} &= \int (W^{(1,2)} n_x - T_i^{(1)} \frac{\partial u_i^{(2)}}{\partial x} - T_i^{(2)} \frac{\partial u_i^{(1)}}{\partial x}) ds \end{aligned} \tag{2.11}$$

where $W^{(1,2)} = \sigma_{ij}^{(1)} \epsilon_{ij}^{(2)} = \sigma_{ij}^{(2)} \epsilon_{ij}^{(1)}$ is the interaction strain energy density and $T_i = \sigma_{ij} n_j$ is the traction.

The superposed SIFs from Equation (2.9) are then inserted into Equation (2.7) to obtain the second $M$-integral formulation denoted with subscript 2:

$$J_2 = J_2^{(1)} + J_2^{(2)} + M_2^{(1,2)} \tag{2.12}$$

where the interaction term $M_2^{(1,2)}$, now in terms of the SIFs, is expressed as follows

$$M_2^{(1,2)} = \frac{2 K_{\mathrm{I}}^{(1)} K_{\mathrm{I}}^{(2)}}{E'} + \frac{2 K_{\mathrm{II}}^{(1)} K_{\mathrm{II}}^{(2)}}{E'} + \frac{2(1+\nu) K_{\mathrm{III}}^{(1)} K_{\mathrm{III}}^{(2)}}{E} \tag{2.13}$$

The auxiliary states are then defined such that one solution is obtained for each pure mode, according to Equation 2.14.

$$(K_{\mathrm{I}}^{(2)}, K_{\mathrm{II}}^{(2)}, K_{\mathrm{III}}^{(2)}) = \begin{cases} (1,0,0) & \text{Pure mode I} \\ (0,1,0) & \text{Pure mode II} \\ (0,0,1) & \text{Pure mode III} \end{cases} \tag{2.14}$$

Three corresponding values of the first $M$-integral formulation are then obtained from Equation (2.11) in combination with the solutions to the stress and displacement fields in Equation (2.2) and (2.4). These values are denoted $M_{\mathrm{I}}^{(1,2)}$, $M_{\mathrm{II}}^{(1,2)}$ and $M_{\mathrm{III}}^{(1,2)}$, for pure mode I–III respectively. The SIFs can then be evaluated from Equation (2.13) resulting in the following expressions

$$K_{\mathrm{I}}^{(1)} = \frac{E'}{2} M_{\mathrm{I}}^{(1,2)}, \quad K_{\mathrm{II}}^{(1)} = \frac{E'}{2} M_{\mathrm{II}}^{(1,2)}, \quad K_{\mathrm{III}}^{(1)} = \frac{E}{2(1+\nu)} M_{\mathrm{III}}^{(1,2)} \tag{2.15}$$

The $M$-integral in Equation (2.11) is on a form not well suited for FE-calculations. A technique can be employed in order to formulate the integral as an equivalent domain integral which is more compatible with FEM. This is done by introducing a weight function $q$ called the virtual crack extension. For more on this topic, see [9, 10, 11].

### 2.2.4 Numerical evaluation of $M$- and $J$-integral

In a continuous body, the $M$- and $J$-integrals can be evaluated as described in the previous two sections. It is also is possible to transform the surface integral, as seen in Equation (2.6), into a domain integral which is more suitable for numerical integration, see for instance Gauss quadrature method for numerical integration [13]. A typical domain of integration in 3D is illustrated in Figure 2.4. The integration is carried out within the tubular volume enclosed by the inner and outer surfaces.

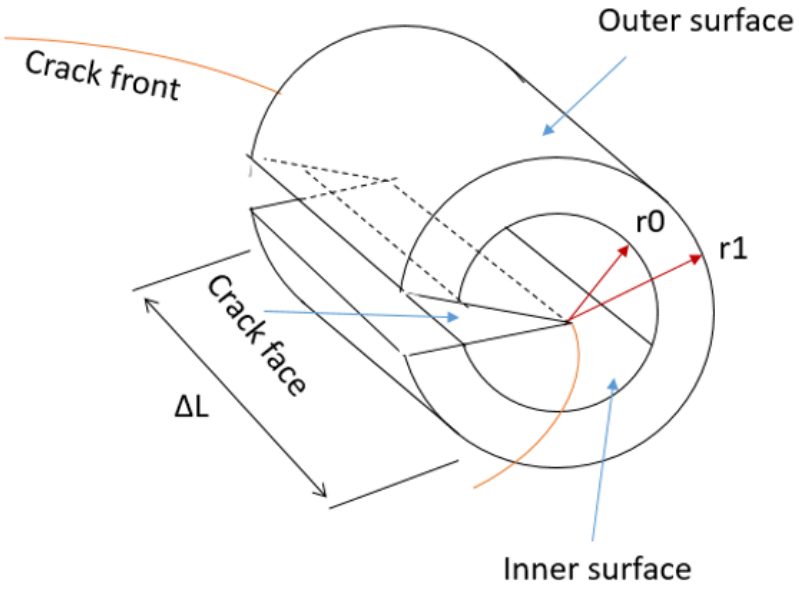


**Figure 2.4:** Integration domain with volume $V^*$ used for evaluation of $M$- or $J$-integral,

Several domains as seen in Figure 2.4, surrounds the crack front. The SIFs are

evaluated within each of these tubular shaped domains. The summation of Gauss points over each tube evaluates the $J$-integral, as employed in Equation (2.16). This presumes the absence of traction at the crack surface. A weighted summation is carried out over the tube volume $V^*$, as defined in Figure 2.4. where $m$ is the number of Gaussian integration points within $V^*$, $w_p$ the Gauss point weights and the determinant expression corresponds to the area size transformation between the spatial and iso-parametric elements.

$$J = \sum_{V^*} \sum_{p=1}^{m} \left\{ \left[ \left( \sigma_{ij} \frac{\partial u_j}{\partial x_1} - W \delta_{1i} \right) \frac{\partial q}{\partial x_i} \right] det\left( \frac{\partial x_j}{\partial \xi_k} \right) \right\}_p w_p \tag{2.16}$$

Both the $J$- and $M$-integral are path independent for LEFM, as shown in [12] for the $J$-integral. This property is naturally extended to the $M$-integral since it is made up of superposition of $J$-integral expressions. This means that it is not necessary to integrate within the elements closest to the crack front. In e.g. ANSYS one can define a number of contours making up several tubes with different sizes to have the integration performed for more than one tube size. If tubes with elements having nodes that coincide with crack front is chosen for integration it is necessary to include another type of element, that is made by collapsing the mid side node to the quarter point of a wedge element in order to capture the singularity behaviour near the crack front [3, p. 586].

Anderson [3, p. 586-589] describes a methodology on how to generate a convenient mesh for SIF evaluation. An example of such a mesh, for a 2D case, is seen in Figure 2.5. Around the crack tip a more dense mesh is constructed similar to a spider's web, while further away the mesh is coarse.

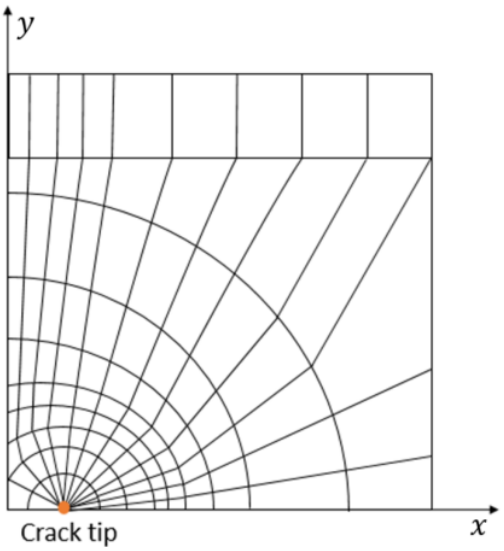


**Figure 2.5:** 2D mesh, with symmetry about the x-axis, that illustrates a convenient mesh for SIF evaluation around the crack tip. The area integration is carried out within adjacent contours

## 2.3 Crack propagation

The main driving force affecting the fatigue crack growth rate is the range of the SIF, $\Delta K$ [5, p. 564]. The crack growth rate as a function of $\Delta K$ can be divided into three regions as shown in Figure 2.6.

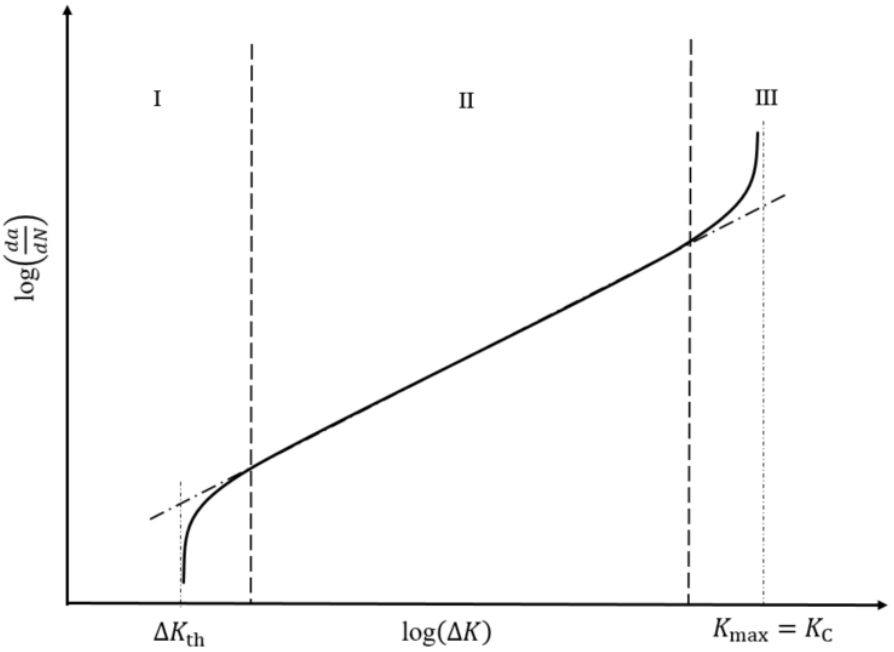


**Figure 2.6:** Illustration of the crack growth rate versus the SIF range divided into three regions

For intermediate $\Delta K$ values, illustrated as region II in Figure 2.6, the curve is linear. The linear part of the log–log plot can be described by a power law widely known as the Paris law

$$\frac{\mathrm{d}a}{\mathrm{d}N} = C\Delta K^m \tag{2.17}$$

where $m$ and $C$ are material constants obtained from experiments [3, p.517]. The SIF range is defined as the difference between the maximum and minimum SIFs for each cycle as follows: $\Delta K = K_{\max} - K_{\min}$ [5, p. 564].

In region I there exists a threshold value $\Delta K_{\mathrm{th}}$ which implies that fatigue cracks will not propagate for $\Delta K$ magnitudes below this value. It is difficult to predict crack propagation in this region due to a large influence of both microstructure and mean stress. An increased sensitivity to stress history and environmental effects have also been observed in this region [14]. Extending Paris law (Equation (2.17)) to this region will often lead to an overestimation of the crack growth, it is therefore necessary to find other models that can capture the behaviour in region I.

In region III, $\Delta K$ is very high, the crack growth rate accelerates and becomes infinite as $K_{\max}$ approaches the critical stress intensity $K_{\mathrm{C}}$. At this point fracture will occur.

In this region the crack growth rate becomes extremely sensitive to microstructure and mean stress [14]. In this case extending Paris law results in an underestimation of the crack growth, it is there necessary to find models that capture this accelerating crack growth behaviour in this region.

### 2.3.1 Effects of load ratio on fatigue crack growth

The stress ratio, commonly denoted as the $R$-ratio, is defined as $R = S_{\min}/S_{\max} \equiv K_{\min}/K_{\max}$. It is observed from experiments that the $R$-ratio affects the growth rate, and an increase in the absolute value of the $R$-ratio causes the growth rate for a given $\Delta K$ to be larger [5, p.574].

In order to capture these $R$-effects or mean stress effects on the crack growth rate ($\mathrm{d}a/\mathrm{d}N$) we introduce the Walker equation and modify the SIF range as follows

$$\overline{\Delta S} = S_{\max}(1-R)^{\gamma} \tag{2.18}$$

$$\Rightarrow \overline{\Delta K} = K_{\max}(1-R)^{\gamma} = \frac{\Delta K}{(1-R)^{1-\gamma}} \tag{2.19}$$

where the Walker exponent $\gamma$ is a material constant and $\overline{\Delta K}$ is an equivalent zero-to-tension stress intensity factor range. The constant $C$ in Paris law (Equation (2.17)) is now denoted $C_0$ for the special case $R = 0$ and $\overline{\Delta K}$ is substituted for $\Delta K$. The modified crack growth equation, according to [5, p. 575], then takes the form

$$\frac{\mathrm{d}a}{\mathrm{d}N} = C_0(\overline{\Delta K})^m = \frac{C_0}{(1-R)^{m(1-\gamma)}}(\Delta K)^m \tag{2.20}$$

$$C = \frac{C_0}{(1-R)^{m(1-\gamma)}} \tag{2.21}$$

Compared to Equation (2.17), $C$ now becomes a function depending on $R$ as expressed in Equation (2.21). In a log–log plot the crack propagation rate plotted against the SIF range will all be parallel lines with slope $m$, but shifted to the left for increasing $R$-ratios.

### 2.3.2 NASGRO crack propagation model

Several crack propagation models have been developed over the years to improve prediction accuracy and incorporate a variety of effects such as R-ratio, overloads and load history effects. In this thesis work, the NASGRO equation will be used for modelling the crack propagation. The NASGRO equation is more accurate than the standard Paris law, in the sense that it includes lower growth rates near the threshold and increased growth rates near $K_{\mathrm{C}}$. The NASGRO equation also accounts for mean stress effects and is defined as

$$\frac{\mathrm{d}a}{\mathrm{d}N} = C\left[\frac{(1-f)}{(1-R)}\Delta K\right]^n \frac{(1-\frac{\Delta K_{\mathrm{th}}}{\Delta K})^p}{(1-\frac{K_{\max}}{K_{\mathrm{C}}})^q} \tag{2.22}$$

where $f$ is the crack opening function and $C, n, p, q$ are empirically derived constants. The SIF is calculated based on load case(s) and geometry as described by Equation (2.5). Expressions for $\Delta K_{th}$, $K_c$ and $f$, can be found in [8]. For illustration, the crack opening function, $f$, as a function of the stress ratio is seen in Figure 2.7.

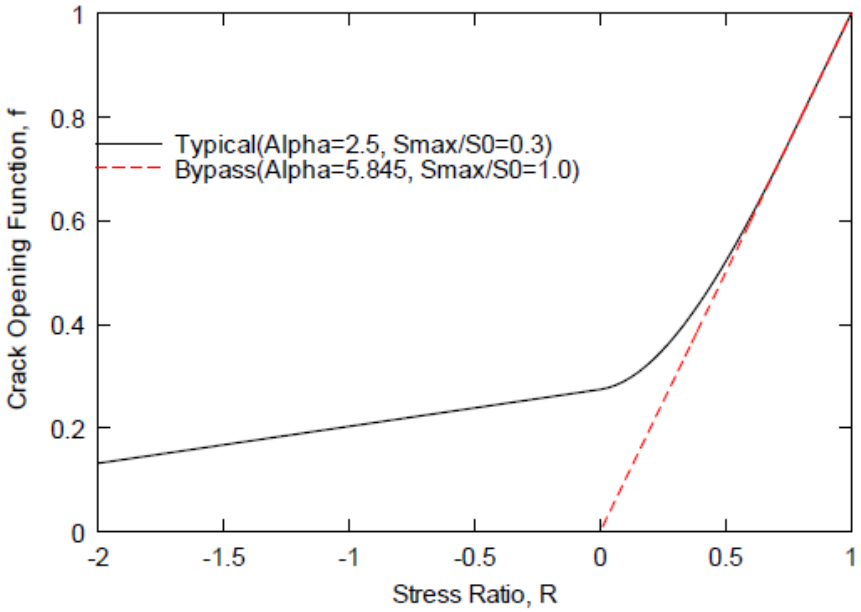


**Figure 2.7:** Illustration of crack opening function. Taken from [8]

## 2.4 Crack propagation testing

For validation of the numerical methods, previously conducted crack propagation tests of Kb test specimens were considered for two different load cases: tensile loading and four-point bending. Figure 2.8 shows an illustration of the test specimen as mounted in the test machine. The dimensions of the specimens vary slightly from specimen to specimen, average values of the width and thickness were therefore used in the simulations. The mean size of the cross section was 4.30x10.16 mm and the height was set to 20 mm.

The testing procedure was divided into three stages: pre-cracking, crack growth and fracture. A notch is located in the middle of the specimen and the pre-crack is obtained from tensile pre-fatigue loading to obtain a sharp crack with its front outside the influence zone of the notch. The crack grows under tensile or bending fatigue until the final crack sizes are reached. Fracture is obtained by either a monotonic bending or monotonic tension load. The fatigue crack size as a function of cycles are obtained from a combination of potential drop technique and heat tinting.

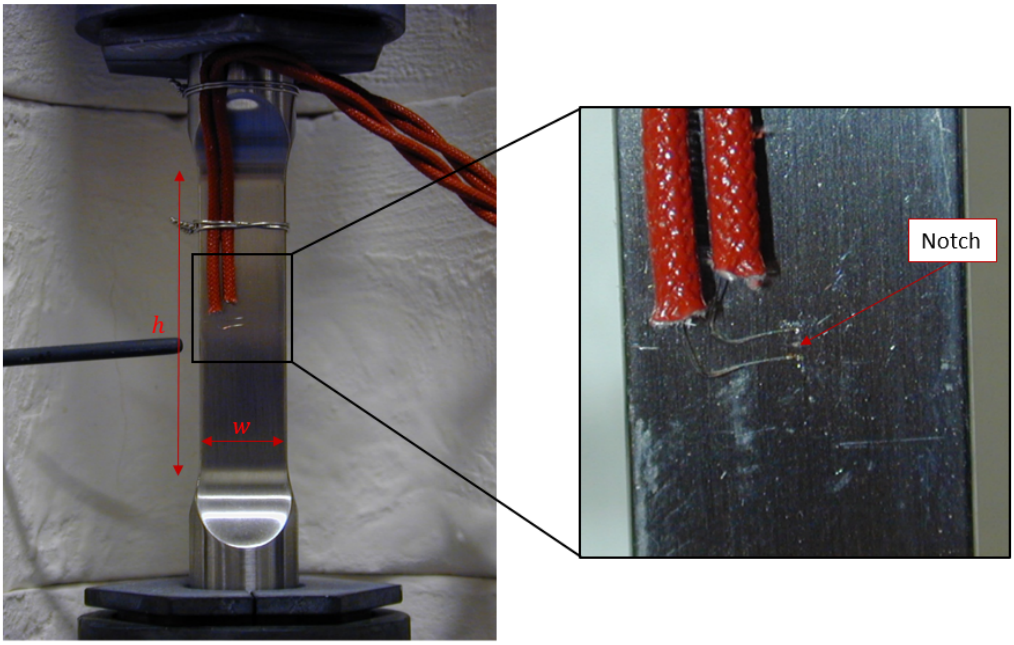


**Figure 2.8:** Illustration of Kb test specimen mounted in test machine. A notch is located in the middle of the specimen, as seen to the right

### 2.4.1 Tensile loading

A schematic illustration of the loading in a tensile test is seen in Figure 2.9. Both ends of the test specimen are mounted into the test machine. During the test one end is kept fixed while a load is applied on the other end. The initial surface crack, after pre-cracking, is located in the middle of the specimen so that the load acts in Mode I.

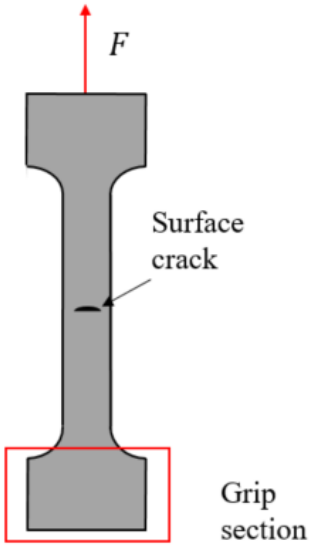


**Figure 2.9:** Schematic illustration of crack propagation test specimen under tensile/compressive loading

### 2.4.2 Four-point bending loading

Figure 2.10 shows a schematic illustration of the loading for a four-point bending test. The specimen is placed between two pairs of rollers. The total force $F$ is applied and equally distributed to the pair of rollers at the top, while the crack is located at the bottom surface in the middle of the specimen. This test is similar to the 3-point bending test. The major benefit of adding a fourth roller is that the portion of the specimen between the two loading points is put under maximum stress, while for 3-point bending only the material under the roller at the centre is affected. For this setup only $R = 0$ was considered.

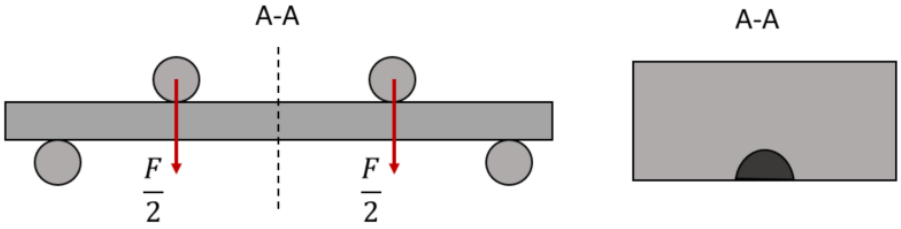


**Figure 2.10:** Schematic illustration of crack propagation test specimen under four-point bending

# 3

# Simulation Method

## 3.1 Simulation process in FRANC3D

The simulation process in FRANC3D is divided into 5 steps, it is illustrated as a flow chart in Figure 3.1. The first three steps consider the setup of the problem by importing the uncracked FE-model, inserting the crack and specifying the crack growth parameters. During the last two steps the analysis is preformed and relevant results post processed. The different steps are described more in detail in sections 3.1.1–3.1.4.

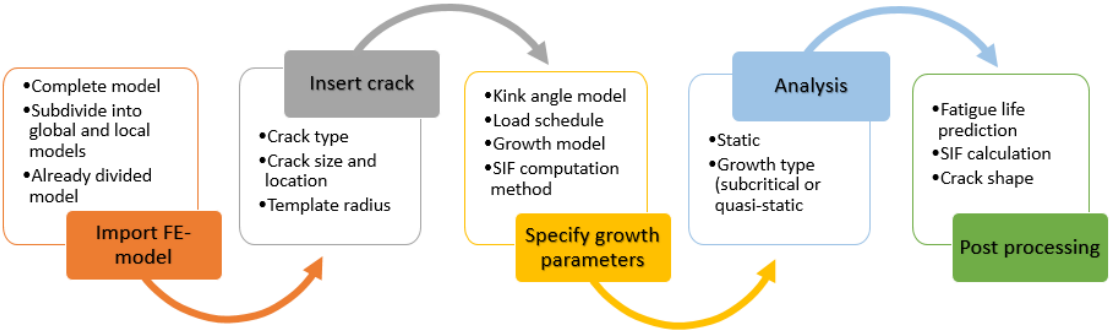


**Figure 3.1:** Flow chart illustrating the simulation process in FRANC3D

A script was created in Matlab to automate the simulation process so that the simulations could be preformed in batch mode instead of using the GUI. This was done in order to reduce the time needed to perform the initial three steps (import FE-model, insert crack and specify growth parameters). This made it possible to perform a large amount of analyses for various initial crack sizes, growth parameters and/or applied loads. More details about this script is presented in section 3.1.5.

### 3.1.1 Import FE-model

ANSYS was used for the initial setup of the FE-model. Boundary conditions, applied loads and the global mesh were prescribed and exported as a *.cdb* file, which is an ANSYS database file in ASCII format. The FE-model was then imported into FRANC3D. For larger models or for more complex geometries, it is possible to

include the crack in a local sub-model. The crack insertion and re-meshing is then only applied to the local model. FRANC3D generates an updated input file for ANSYS, with the new mesh after crack insertion, where it combines the local sub-model and the global model. This input file is used by ANSYS to solve the resulting FE-equations.

### 3.1.2 Crack insertion

The initial crack was inserted after importing the FE-model. Different crack shapes are available, but for this thesis work an elliptical crack with one crack front was considered (top left icon in Figure 3.2a). This crack shape can be used for both surface and embedded cracks. It is also possible to insert multiple cracks and insert material defects such as voids. The crack is then incorporated into the uncracked model at the desired location, see Figure 3.2b, after defining the initial crack size.

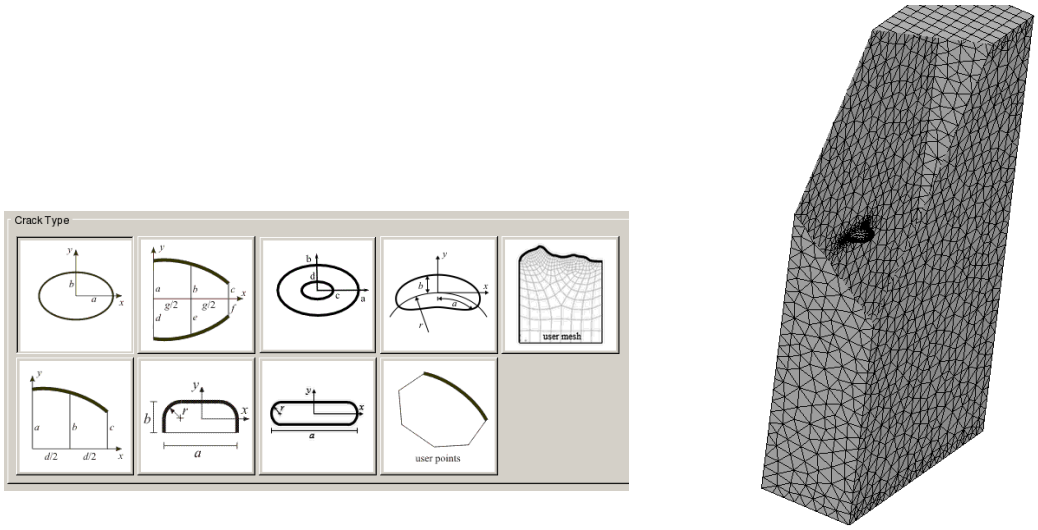


**(a)** **(b)**

**Figure 3.2:** (a) Available crack types and (b) the inserted crack in FRANC3D

### 3.1.3 Crack growth prediction

The crack growth prediction process was divided into five steps, following [15]. First the SIFs were computed for all node points along the crack front. Then the magnitude of the crack front extension and direction of the growth were evaluated. In order to predict the local direction of the crack growth, the Maximum Tensile Stress criterion was used as default. Only Mode I loading was considered in this thesis work, so planar growth is sufficient to chose in this case. A curve was fitted through the newly predicted crack front points and extrapolated, if necessary, to extend outside of the model in order to create a closed curve for re-meshing. A new surface mesh, consisting of Bézier patches (more on that topic can be found in [16]), was created on the crack surface and the new extended crack inserted and connected to the uncracked mesh.

The amount of median extension and the front fitting type were specified, as shown in 3.3a, while the size of the template radius was specified according to Figure 3.3b.

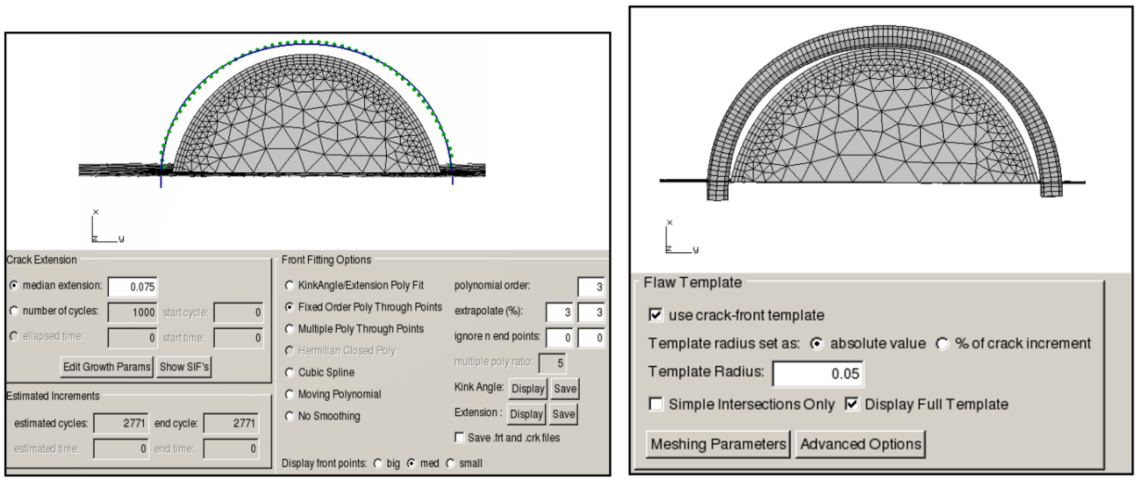


**(a)** **(b)**

**Figure 3.3:** Settings for crack growth analysis: (a) Extension and front fitting and (b) template radius

### 3.1.4 Extraction of results

There are different ways to extract or plot the predicted fatigue life. One way is to extract the number of cycles required to grow the crack from one size to another. An alternative to this is to define paths through the predicted crack fronts as illustrated in Figure 3.4. This makes it possible to plot the number of cycles, or alternatively $K$ versus the crack length along the defined paths.

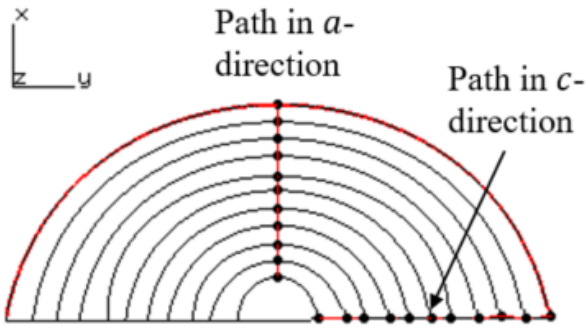


**Figure 3.4:** Paths (marked by dotted lines) used for extracting the predicted fatigue life. One path defined in the $a$-direction and one in the $c$-direction

### 3.1.5 Automating FRANC3D simulations

Many test cases were considered and the test cases were different with respect to applied force, stress ratio, initial crack size, temperature, etc. In order to automate the simulation process, a Matlab script was created. The purpose of this script was to generate and modify *.cdb* and *.log* files from tabulated values for each test case. In the *.cdb* file the applied load was changed so that it corresponds to the load for the actual test case. Then the crack propagation settings in the *.log* file that are used as input to FRANC3D were modified and the initial crack size specified. The modified *.cdb* file was then called from the *.log* file.

After creating these input files, they were executed automatically from the Matlab command window in batch mode. The output files were saved in a predefined folder. The main benefit of running simulations in batch mode is that input data and settings can be specified in the Matlab script instead of manually typing these in through the GUI. This reduces the time needed to run and prepare each simulation and makes it possible to run simulations for a large amount of test cases automatically using a computational cluster.

## 3.2 Simulation process in NASGRO

NASGRO provides a variety of crack cases for fracture analysis. These cases are mainly based on FEA- or BEM-solutions for SIF calculation [8]. As outlined in Equation (2.22), $K$ depends on the geometry and the load type specified by the particular crack case. NASGRO has only the possibility to evaluate the Mode I SIF, i.e $K_{\mathrm{I}}$.

The simulation process in NASGRO is outlined in Figure 3.5. In the first step the simulation type is chosen, for this thesis work the simulation modules were limited to NASSIF and NASFLA. The NASSIF module calculates stress intensity factor solutions and the NASFLA module calculates fatigue crack growth rates at points defined by NASGRO for the particular crack. In the NASSIF module one has to chose the crack case and then define load(s) and initial crack size. An example of a crack case is outlined in section 3.3.

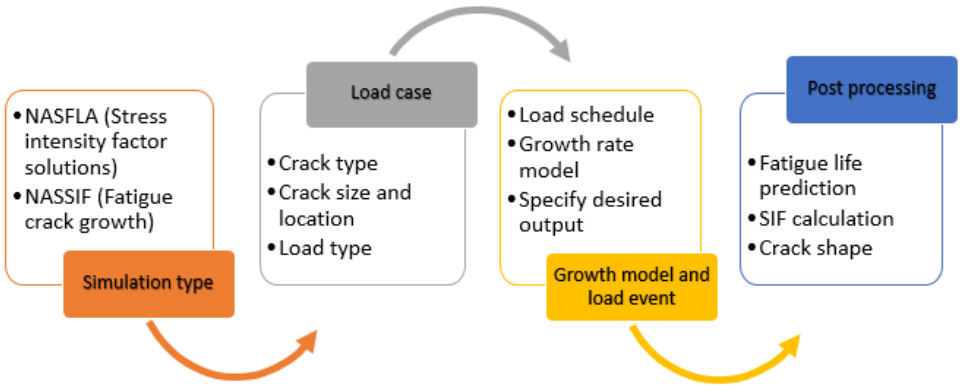


**Figure 3.5:** Chart showing the steps for a NASGRO simulation used in this thesis

In the NASFLA module the SIF is calculated based on load case, crack geometry and load magnitude defined from the load schedule. By use of the calculated SIF the crack growth is determined by the crack propagation law, e.g the NASGRO equation as used in this thesis, see Equation (2.22). The SIFs are then evaluated for the new crack geometry and the process continues repeatedly until the crack has grown to a desired length or width, as specified in the output options, or if the simulation results meet a failure criterion. In this thesis, the fracture toughness $K_{\text{cr}}$ has been used as the only failure criteria, which is calculated dependent on crack case, see [8, Appendix U].

### 3.2.1 Semi-elliptical surface crack

Mainly semi-elliptical surface cracks have been investigated and the proceeding text will therefore focus on these types of cracks. NASGRO calculates the SIFs at two points along the crack front, as seen in Figure 3.6. NASGRO predicts how much the crack will propagate at those points from the provided crack propagation model with a cycle by cycle routine or by updating the crack growth rate at a user defined increment size and then integrate the interpolated values between the increments, An elliptical fitting between the crack growth points is then made. $K$ at the position c is taken as the maximum value close to the free surface of the crack front, usually three degrees in from the free surface for the semi-elliptical surface crack [8, p.245, Appendix C].

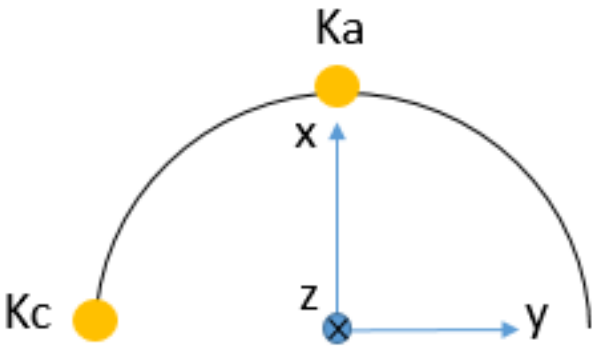


**Figure 3.6:** Points where NASGRO assigns $K$ values and predicts crack growth

Observations from experiments have shown that the crack grows less at the surface (point c in Figure 3.6) compared to the calculated growth [8, p.11]. To adjust for this, a factor $\beta$ is introduced that reduces the growth at the surface. This factor is taken as $\beta = 0.9$ for $R \leq 0$ and $\beta \in [0.9, 1]$ for $0 \leq R \leq 1$ [8], where $\beta$ is linearly increasing for higher $R$ values for which the crack grows slower.

## 3.3 Three-way comparison of SIF evaluation for a surface crack

In order to investigate the ability of three different programs, (FRANC3D, ANSYS and NASGRO) to evaluate SIFs, a study was performed for a simple test case. The investigation was performed to compare the Mode I SIFs along the crack front for static tensile loading. The case corresponds to NASGRO SC30 crack type as shown in Figure 3.7, with geometry and load as defined in Table 3.1. The corresponding FE-models that was used in ANSYS and FRANC3D is described in the following sections.

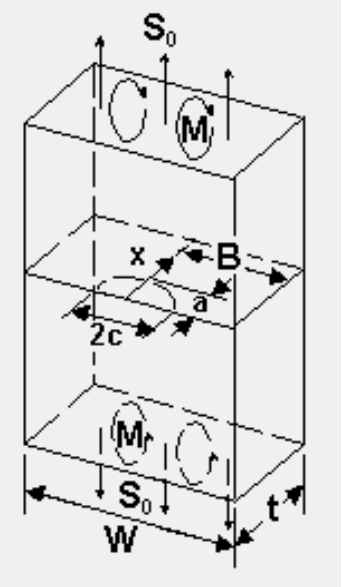


**Figure 3.7:** Surface crack in a plate (Case SC30 in NASGRO) [8, Appendix C]

**Table 3.1:** Plate and crack geometry parameters used in the comparison for a surface crack

| $S_0$ | $W$ | $t$ | $B$ | $a$ and $c$ |
|---|---|---|---|---|
| 100 MPa | 20 mm | 6 mm | 10 mm | 0.76 mm |

### 3.3.1 Modelling of FE-specimen in ANSYS

In the ANSYS model, as shown in Figure 3.8, a symmetry condition was applied at the crack plane. The ANSYS model has boundary condition $u_z = 0$ at the symmetry plane except were the crack surface is located. In addition $u_x = u_y = 0$ for one node at the corner (marked in the right part of Figure 3.8). The pressure load is applied to the top surface.

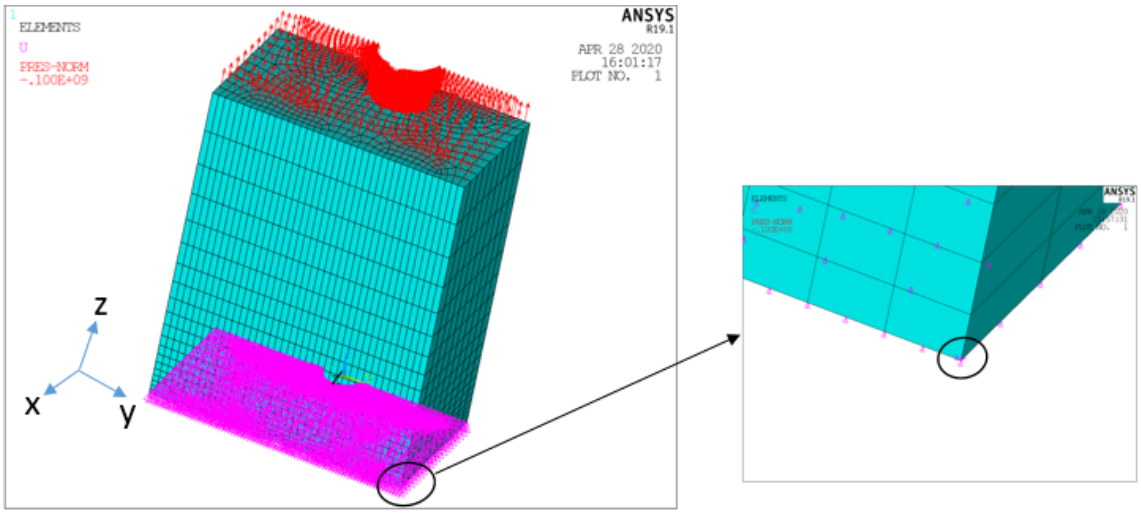


**Figure 3.8:** ANSYS model with boundary conditions (magenta colour) at the symmetry plane and pressure load (red colour)

### 3.3.2 Modelling of FE-specimen in FRANC3D

The FRANC3D model used the full size model defined in ANSYS. The crack was inserted as described in section 3.1.2. The FE-model used in FRANC3D is seen in Figure 3.9. The FRANC3D model had the B.C. $u_z = 0$ at the whole bottom surface. The FRANC3D model had in addition to the ANSYS model, also one additional node constrained with $u_x = 0$ to prevent RBM. The applied B.C. is seen in the bottom left and right part of Figure 3.9, where node $C_1$ is locked in x- and y-direction and node $C_2$ is locked in x-direction. The applied pressure load is seen at the top of the model, in the top left part of Figure 3.9.

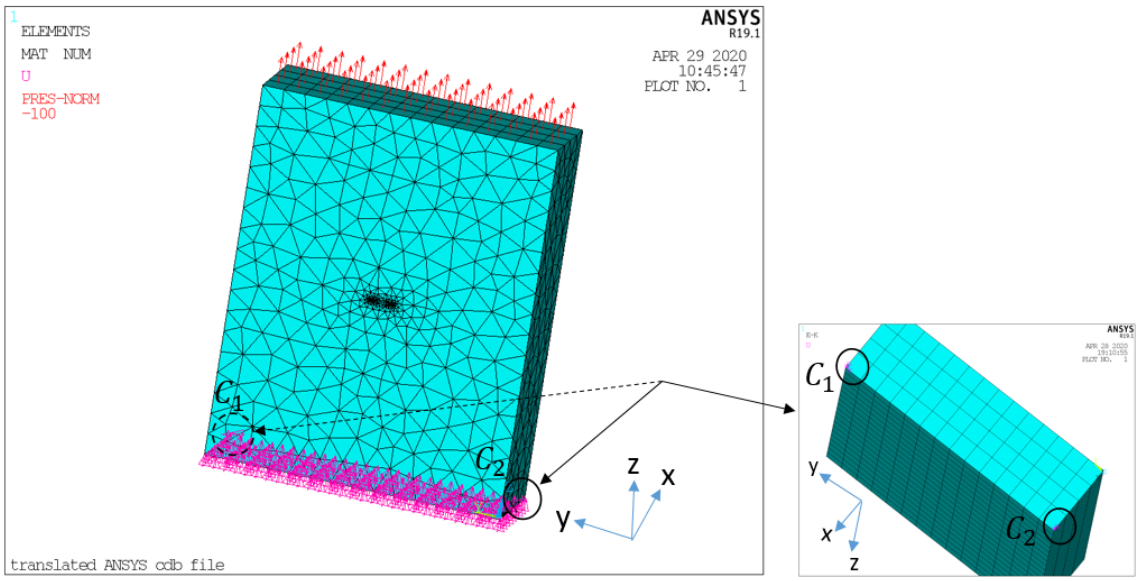


**Figure 3.9:** FRANC3D model with boundary conditions (magenta colour) and pressure load (red colour)

#### 3.3.2.1 Domain integration in ANSYS

To obtain an accurate model in ANSYS a mesh that was conjugate to how the domain integration is performed was needed. The ANSYS manual [17] describes how to perform the domain integration in the program. The numeric integral is evaluated along the user specified crack front, as described in section 2.2.4. The user has to supply information to the ANSYS CINT command to carry out the SIF calculation. The following information are needed for the SIF calculation: the normal to the crack plane, a component of nodes that constitute the crack front, numbers of contours to integrate within and if a symmetry condition is used.

A schematic view of the contours surrounding the elements used can be seen in Figure 3.10, with the mesh topology as used in this test case for ANSYS. The contours seen in Figure 3.10 are increasing in size when moving out from the crack front nodes. Every new contour makes up the new integration volume together with the previous one. Ideally the integrated values along the different contours should be similar, but ANSYS gets poor result close to the crack front, which is an artefact of the element definition. As described in section 2.2.4 another type of elements is needed at the crack front to capture the asymptotic behaviour of the stresses. Some contours away from the crack front it has been observed that the result is quite stable with the type of mesh topology used in this case.

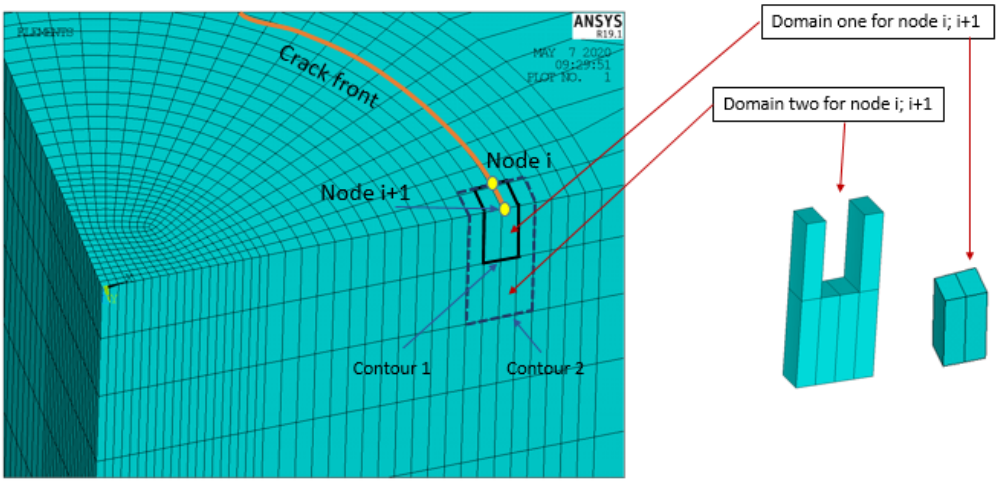


**Figure 3.10:** Integration domains for different contours

### 3.3.3 SIF comparison along crackfront

To investigate whether the solution for ANSYS, NASGRO and FRANC3D become similar, $K_{\mathrm{I}}$ was compared for the models described in the previous section along the crack front. An analytic solution [3, p.627] for a semi-circular surface crack located at the centre of a infinite large plate was used as a reference. The result is seen in Figure 3.11, in this case a fine mesh was used for both FE-analyses. The $K_{\mathrm{I}}$ values are seen to be close for FRANC3D and ANSYS which suggest that either method works in this case. The NASGRO solution is seen to match better at the centre of

the crack front to the analytic solution. In ANSYS one has to define which contour the SIFs are to be extracted from. With a fine mesh as used in this example the variation between the contours is small, except for those closest to and the farthest away from the crack.

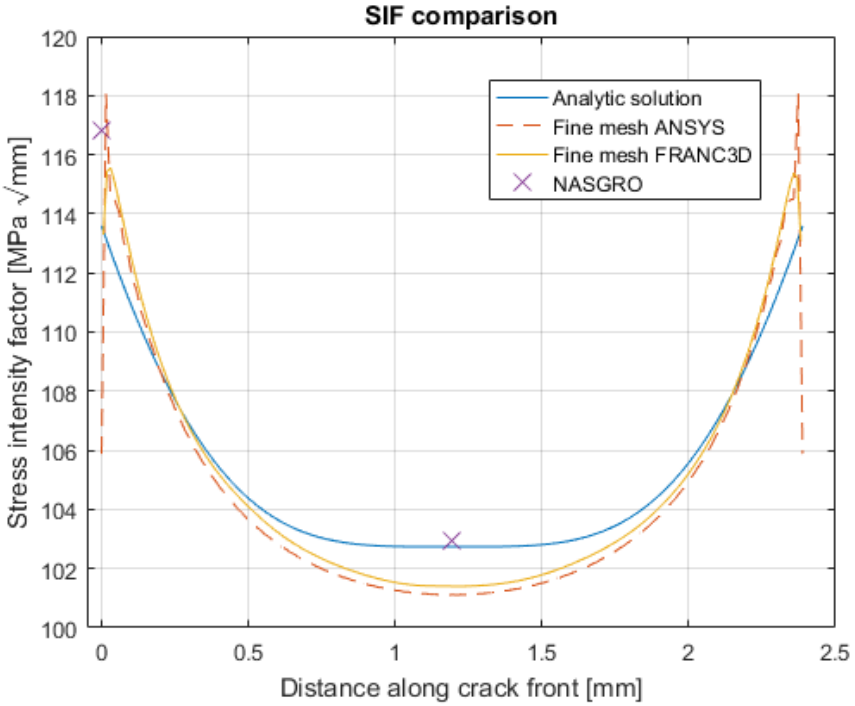


**Figure 3.11:** SIF comparison along crack front between ANSYS, NASGRO, analytic solution and FRANC3D

#### 3.3.3.1 Mesh refinement and SIF computation methods

Figure 3.12 shows the mesh around the crack front including the parameters describing the mesh division for the ANSYS model. The mesh division parameters used gave a organised mesh, the integration domains along the crack front had same size and shape and the elements were aligned parallel to adjacent elements around the crack front, as seen in Figure 3.10. Stress field components were thus extracted in the correct way for SIF evaluation. The mesh was refined in the crack plane by division along R1, R2, R3 and along L. The mesh was denser in the volume direction close to the crack plane than at the boundary where the load was applied, so that the domain integration was carried out over a region with a finer mesh at the crack front.

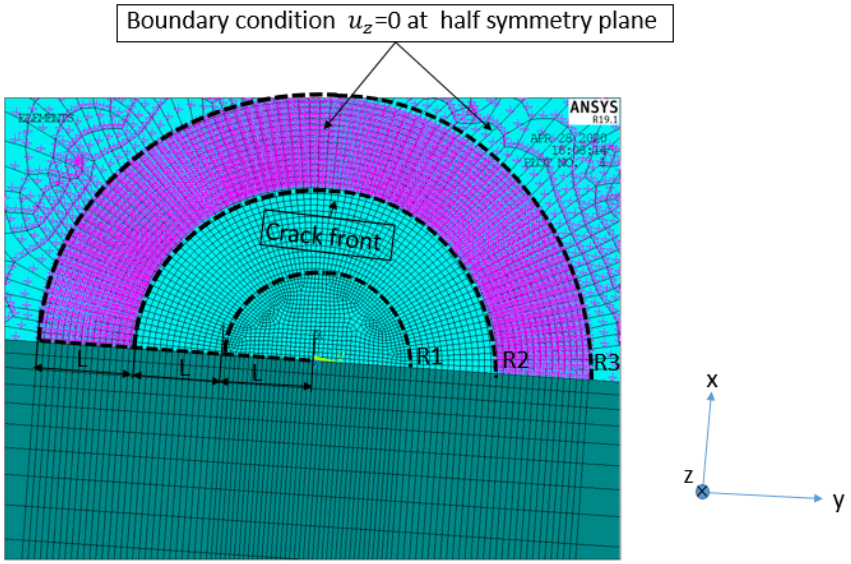


**Figure 3.12:** ANSYS mesh at and around crack front including boundary condition $u_z = 0$ at the half symmetry plane

A mesh sensitivity study was also performed. The mesh topology used in ANSYS is described above and the mesh topology around the crack front in FRANC3D is illustrated in Figure 3.13. $N_r$ is the number of elements in the radial direction within the radius, called template radius. The template radius is defined as the distance were the region of elements surrounds the crack front with the tubular mesh topology. $N_e$ defines the number of elements in the circumferential direction, $\alpha/\beta$ is the progression ratio of the element size in the radial direction, the ratio for $\alpha/\beta$ is the same for all chosen adjacent elements in the radial direction.

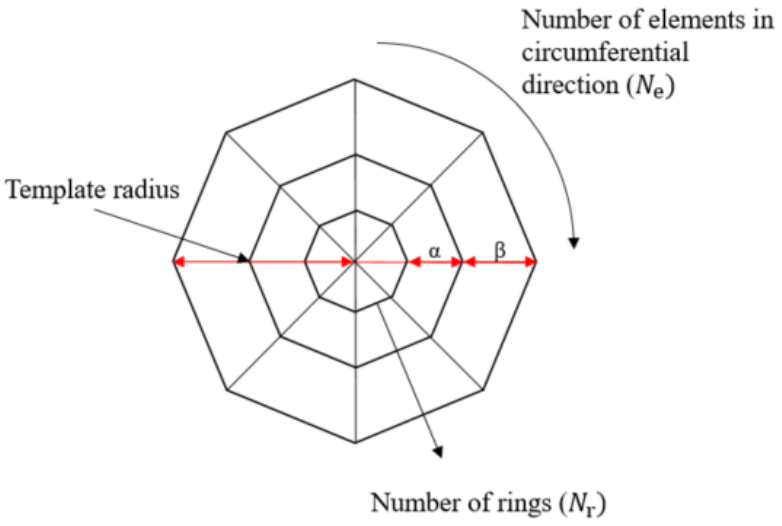


**Figure 3.13:** FRANC3D crack front template mesh. A 2D cut-out of the tube mesh that encloses the crack front

The number of elements used in this study are listed in Table 3.2 for the respective methods. The same mesh topology was used for the 'coarse mesh'. The mesh settings in FRANC3D with respect to number of rings $N_r$ and circumferential divisions $N_e$ were changed to the standard setting to generate the FRANC3D coarse mesh with the listed number of elements. In ANSYS the number of divisions at and around the crack surface was changed and the base mesh refinement was also changed.

**Table 3.2:** Number of elements (NEL) for different meshes

| Mesh | Element divisions | NEL |
|---|---|---|
| ANSYS fine | R1 = R2 = R3 = 40, L = 15 | 64880 |
| ANSYS coarse | R1 = R2 = R3 = 20, L = 8 | 30060 |
| FRANC3D fine | $N_r = 8$, $N_e = 15$ | 103889 |
| FRANC3D coarse | $N_r = 3$, $N_e = 8$ | 16745 |

Both programs gave similar results for the coarser meshes as seen in Figure 3.14, but ANSYS was seen to be unstable with respect to some integration contours. The closest contours around the crack front and the contours furthest away were seen to deviate to those in the middle. There were fewer contours yielding approximately the same results as for the finer mesh.

The influence of SIF computation method in FRANC3D was investigated, as seen in Figure 3.14b. In this case the results were close for the two methods. The displacement correlation method converged with a finer mesh since the method uses the displacements measured at the nodes closest to the crack front straight behind it. For both the coarse and the finer mesh, the displacement correlation method yielded results close to the solution of the M-integral, which suggests that the M-integral is a sound evaluation technique for the SIF. The M-integral method is path independent for LEFM, this makes the M-integral method robust with respect to mesh density as long as the evaluation is carried out over an ordered mesh as used here and the mesh is fine enough to resolve the global stress field and the influence of the crack.

The refined mesh was seen to be smoother around half the crack front distance. Away from that region, the coarser and the finer mesh results are coinciding, except at the crack mouth were the 'finer mesh solution' has larger drops in $K_{\mathrm{I}}$, results in this region does not however provide a physical meaning. A similar behaviour was seen from benchmark tests performed by the FRANC3D authors [18].

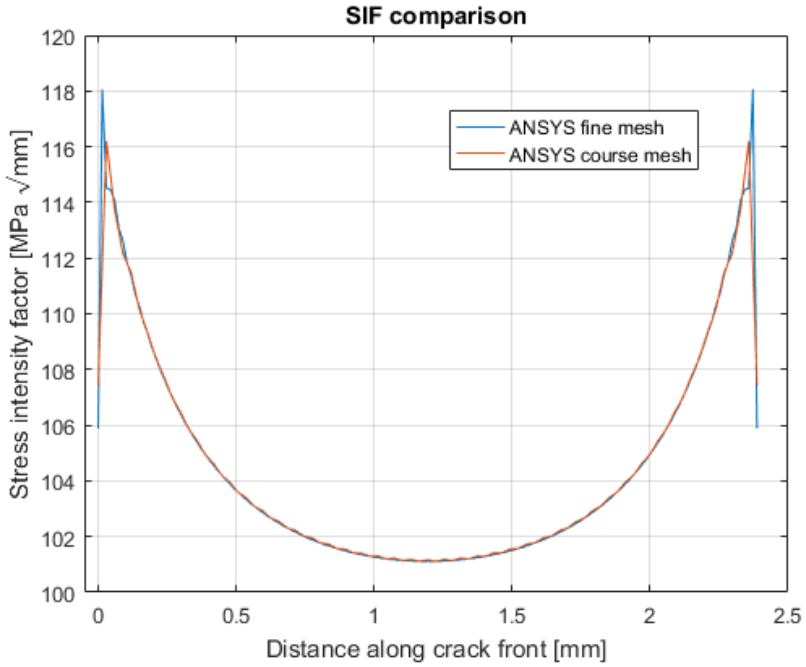


**(a)** SIFs evaluated for different mesh densities in ANSYS

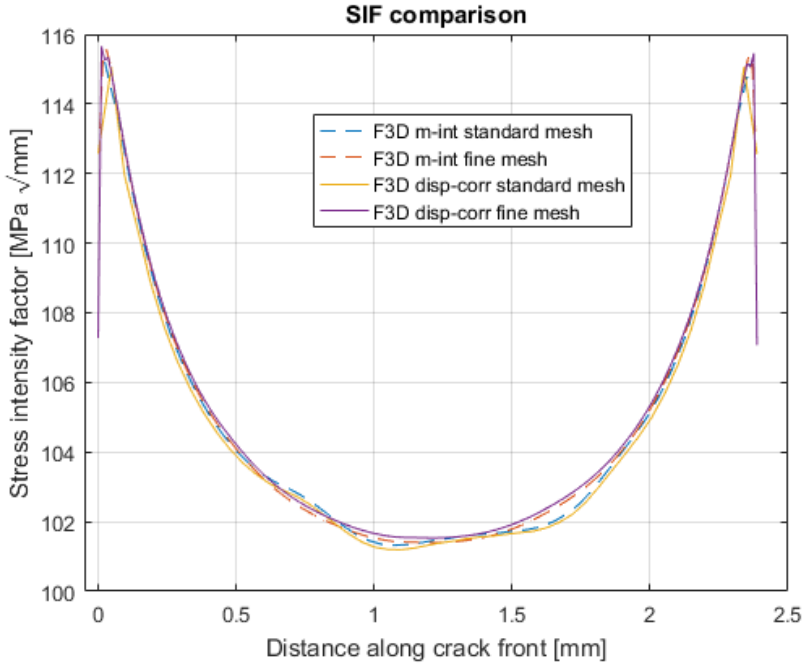


**(b)** SIFs evaluated for different mesh densities and SIF evaluation methods in FRANC3D

**Figure 3.14:** SIF comparison along the crack front. SIF dependency of mesh and $K_{\mathrm{I}}$ evaluation method

## 3.4 Sensitivity study for cyclic tensile loading

Various settings for crack propagation analyses are available within FRANC3D. Information about how these affect the evaluation is limited. In this section different settings regarding e.g. the crack front mesh, the crack growth increment etc. were tested to investigate how these affect the accuracy and stability of the analyses. All simulations in this sensitivity study were performed for Material A. Both semi-circular and semi-elliptical surface cracks were considered. The crack was inserted according to Figure 3.15.

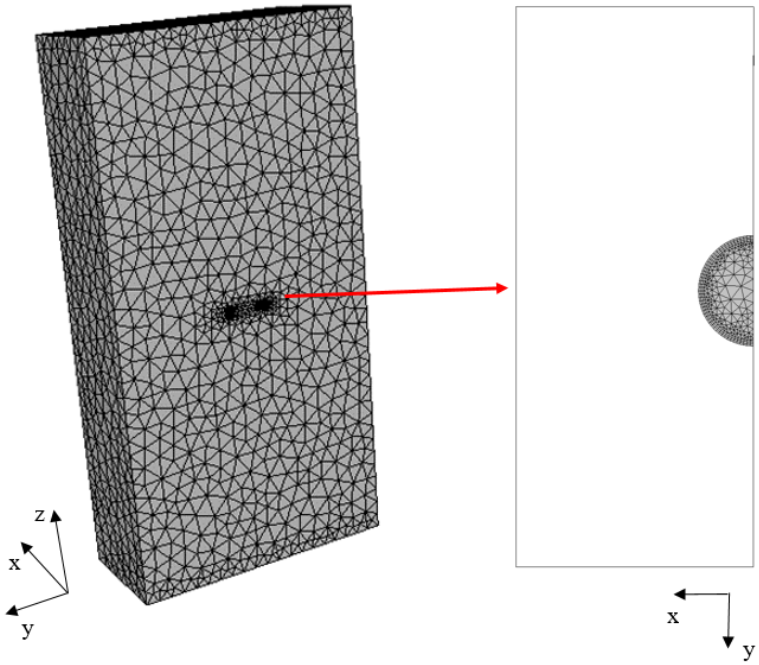


**Figure 3.15:** Illustration of initial crack inserted into FE-model of Kb test specimen performed in FRANC3D

### 3.4.1 Crack growth extension control

In order to control the extension of the crack, FRANC3D provides three different options: median extension, number of cycles, and elapsed time. Only the median extension method was considered in this thesis work, and is used to adjust the amount of crack extension $\Delta a_{\mathrm{m}}$ in each crack growth step. First the SIF range is calculated from the applied load cycle for each point on the current crack front, then the median crack extension $\Delta a_{\mathrm{m}}$ is specified by the user for the point(s) that coincide with median SIF range $\Delta K_{\mathrm{m}}$. The extensions of the remaining points $i$ on the current crack front are then calculated according to Equation (3.1).

$$\Delta a_i = \Delta a_m \frac{\frac{da}{dN_i}(\Delta K_i, R_i, ...)}{\frac{da}{dN_m}(\Delta K_m, R_m, ...)} \tag{3.1}$$

When the new crack front points are evaluated, a curve is fitted through these points to obtain the new predicted crack front as shown in Figure 3.16. To perform the curve fit, several options are available within FRANC3D. Some of these options are studied more in detail in section 3.4.2.

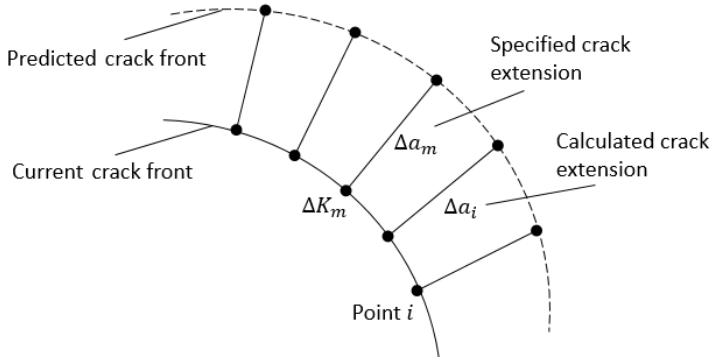


**Figure 3.16:** Median crack extension. Taken from [16]

In order to investigate how the size of the median crack extension affects the crack growth, a semi-circular surface crack with the initial size $a = c = 0.76\,\text{mm}$ was studied (see Figure 3.7). The crack was inserted into a rectangular plate undergoing cyclic zero-to-tension loading. In this study a fixed 3rd order polynomial (default curve fit setting in FRANC3D) was selected as the crack front fitting type. Four crack growth increments were considered varying from $\Delta a_\text{m} = 0.2\,\text{mm}$ to $0.5\,\text{mm}$.

The crack size, in terms of the crack length $a$ and the crack width $c$, was evaluated as a function of $N$ as illustrated in Figure 3.17. The crack size, for both $a$ and $c$, were seen not to be much affected by the increased crack growth extension. There are therefore no clear incentives to choose a very small crack extension in this case. Since will only lead to increased computational time.

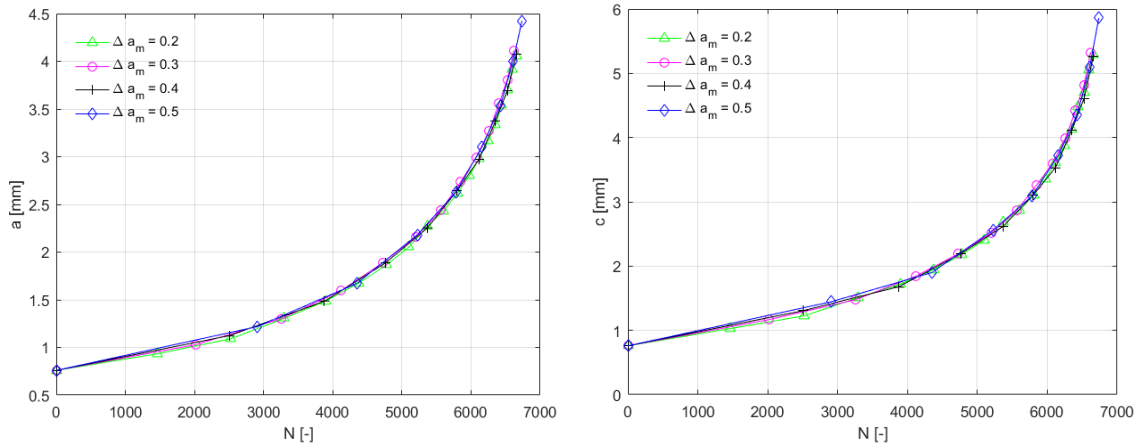


**(a)** **(b)**

**Figure 3.17:** Crack size (a) $a$ as a function of $N$ and (b) $c$ as a function of $N$

The resulting aspect ratio $a/c$ as a function of the crack length $a$ is presented in Figure 3.18. It was observed that the shape of the crack immediately transformed from the initial circular shape to a more elliptical shape. The evolution of the aspect ratios was similar for all the considered median crack extensions, hence the shape of the crack was not very sensitive to crack extensions between $\Delta a_{\mathrm{m}}$ approximately 25% -65% of the initial crack size for the current case.

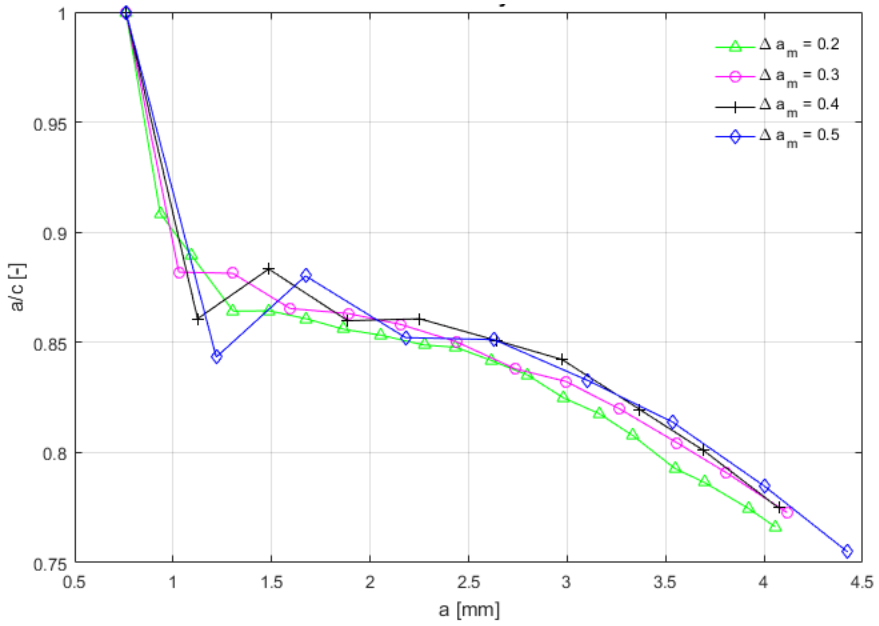


**Figure 3.18:** $a/c$ vs. $a$ for different crack growth increments $\Delta a_{\mathrm{m}}$

### 3.4.2 Crack front fitting

The crack front fitting used initially in this study was a 3rd order fixed polynomial, as seen in Figure 3.19. The same initial crack size was employed as for the crack extension study.

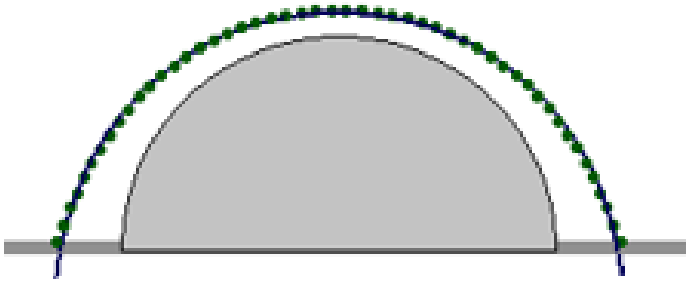

**Figure 3.19:** New predicted crack front based on a 3rd order fixed polynomial fit

For some cases, in particular when the crack becomes wide, a smaller growth is predicted in the $c$-direction near the free surface. This behaviour is illustrated in Figure 3.20. This behaviour was also observed in tests by examination of the fracture surface. The fixed order polynomial resulted in an overestimation of the growth in c-direction. In order to reduce the error other front fitting options were investigated such as a ´´moving polynomial´´ and ´´no smoothing´´.

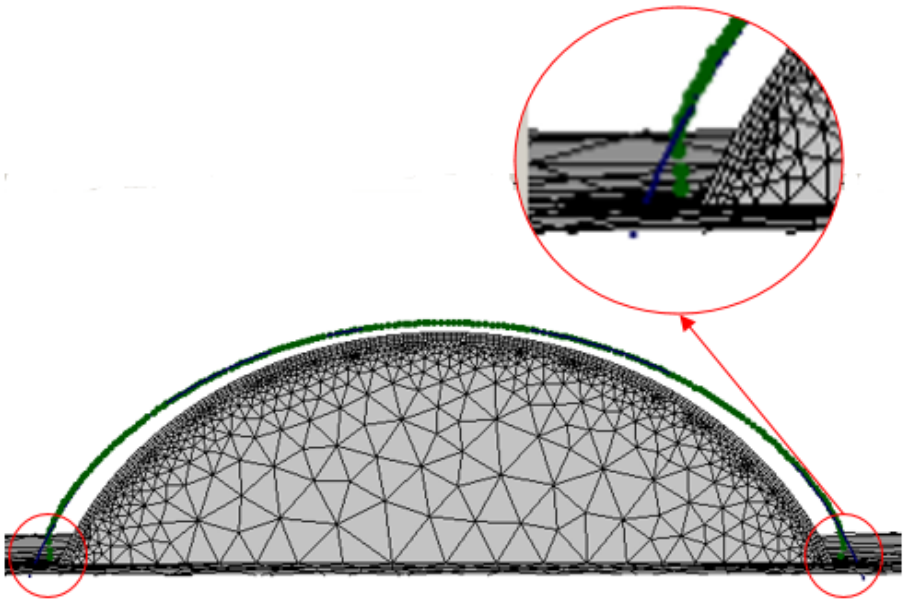

**Figure 3.20:** New front fit that overestimates the growth in $c$-direction. The green dots are predicted from Equation (3.1), while the blue line is the curve fit

The crack seen in Figure 3.20 was propagated one additional step for the two alternative crack front fitting options. The resulting crack fronts are seen in Figure 3.21. The reduced growth in $c$-direction was captured for both options, but for the ´´no smoothing´´ option a more discontinuous crack front was obtained. This may lead to errors due to new predicted crack points overlapping each other. Another observation was that the predicted crack front (blue line in Figure 3.21) this time showed a reduced growth near the surface, but enhanced growth at the surface, cf. Figure 3.20.

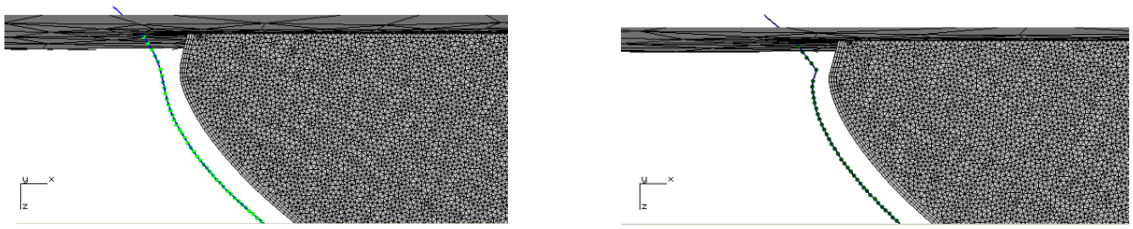

**(a)** **(b)**

**Figure 3.21:** New crack front based on two different front fitting options: (a) moving polynomial and (b) no smoothing

A different amount of extrapolation, see section 3.1.3, was tested in addition to the default 3% extrapolation. This resulted in 5% as a recommended setting to ensure that the predicted crack front intersects with the free surface. It has later been found that large extrapolation also might lead to errors if the new predicted crack front intersects with the old one. The recommendation in that case could be to successively reduce the amount of extrapolation and/or exclude some of the end points until the errors regarding intersection between new and old crack front and/or error creating the new Bezier patch surface crack mesh stop occurring.

### 3.4.3 Mesh refinement around the crack front

A study was conducted for different mesh setting combinations around the crack front in FRANC3D. Only the number of elements in circumferential direction ($N_e$) and the number of rings ($N_r$) were considered in this study, while the template radius and the progression ratio were set to constant values 0.076 mm and 1 respectively (see Figure 3.13). The study was performed for a semi-circular surface crack with length and width $a = c = 0.76$ mm in a Kb test specimen (see Figure 2.9) at $T = 20°C$. The median crack growth extension was set to $\Delta a_m = 0.2$ mm.

In total 9 combinations denoted M1-M9 were considered. The corresponding mesh combinations are shown in Table 3.3. The resulting crack length, width and aspect ratio as functions of $N$ are shown in Figure 3.22 and 3.23 respectively. The results were similar for all mesh combinations, except for the aspect ratio M1 at $N \approx 4300$ cycles. Some mesh combinations led to computational errors related to the re-meshing routine. The crack propagation for M8 and the last part of M6 are therefore not included in Figure 3.23. In order to gain sufficiently accurate results and avoid errors related to the re-meshing routine, the mesh configurations M4 or M6 are recommended.

**Table 3.3:** Combinations of $N_e$ and $N_r$ used in mesh refinement study. These combinations are defined as case ID M1 to M9

| | $N_e = 8$ | $N_e = 12$ | $N_e = 16$ |
|---|---|---|---|
| $N_r = 2$ | M1 | M2 | M3 |
| $N_r = 3$ | M4 | M5 | M6 |
| $N_r = 6$ | M7 | M8 | M9 |

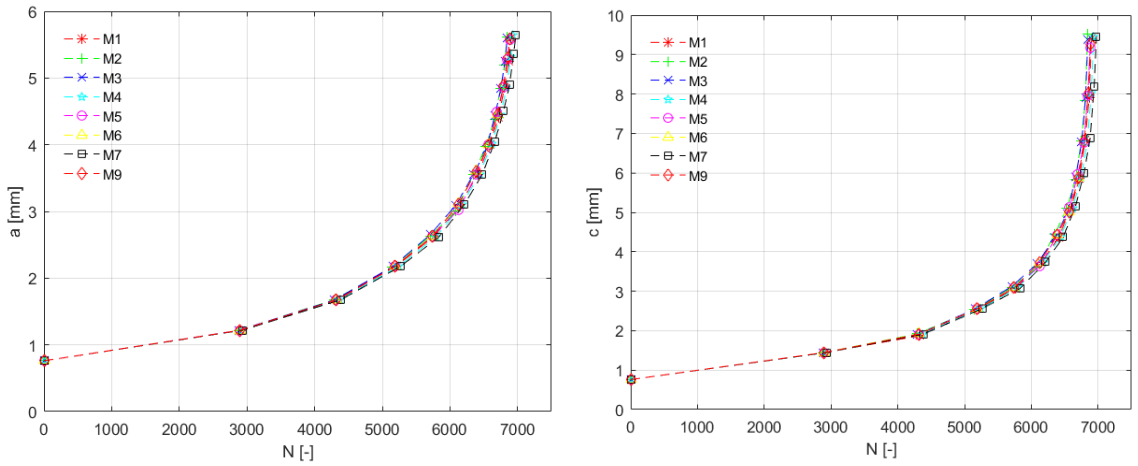


**(a)** **(b)**

**Figure 3.22:** Crack size (a) $a$ as a function of $N$ and (b) $c$ as a function of $N$ for the mesh sensitivity study

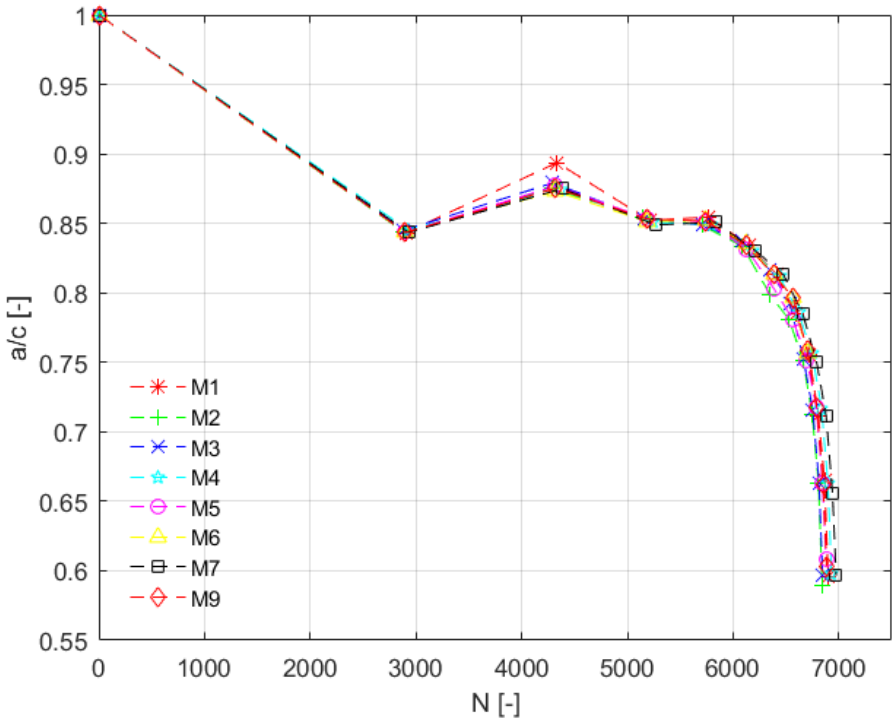


**Figure 3.23:** $a/c$ vs. $N$ for different mesh combinations

### 3.4.4 Mesh-template radius

The template radius as defined in section 3.3.3.1, can be specified either as relative to crack growth increment or as an absolute value. The default is 10% of the smallest crack dimension of the initial crack. To examine the effect of the template radius on the crack propagation simulation results, a semi-elliptical surface crack in a Kb specimen, undergoing cyclic tensile loading, was considered. The initial crack size and applied load is seen in Table 3.4, and the median crack growth was set to $\Delta a_{\mathrm{m}} = 0.5\,\mathrm{mm}$.

**Table 3.4:** Initial crack size and loading for surface crack in Kb test specimen

| $a$ | $c$ | $P_{\max}$ | $R$ | $T$ |
|---|---|---|---|---|
| 0.935 mm | 0.978 mm | 748 MPa | 0.5 | 20°C |

In the first simulation, a relative template radius of approximately 25% of the smallest dimension of the initial crack was specified. This resulted in different SIF values compared to NASGRO, as shown in Figure 3.24a, where SIF is plotted as a function of crack growth. The SIFs were plotted along the growth path in the $a$-direction (see Figure 3.4). In order to improve the accuracy of the predicted SIFs, the relative template radius was changed to an absolute value of 0.05 mm, corresponding to approximately 5% of the smallest initial crack size, which resulted in SIFs closer to the NASGRO solution, as shown in Figure 3.24b. A sufficiently small template radius was therefore decided to be used in all further analyses. It has been experienced that a template radius of approximately 10% of the smallest initial crack size ($a$ or $c$) gives sufficiently accurate SIFs.

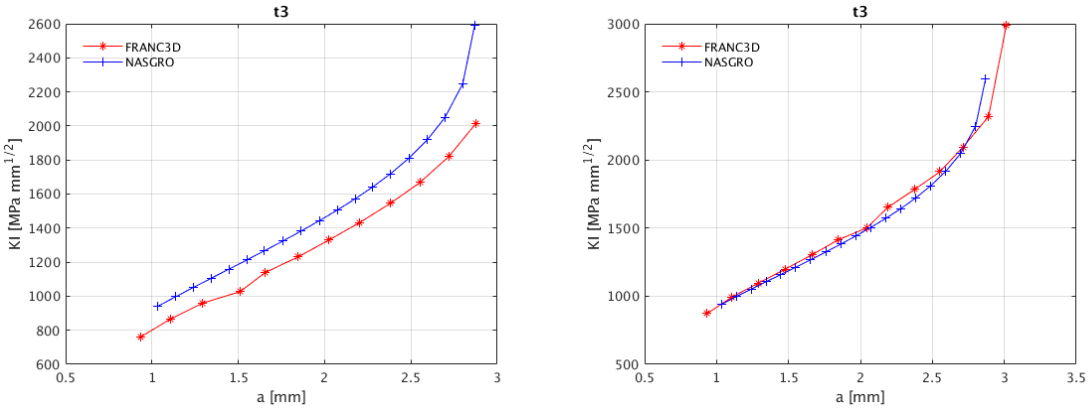


**(a)** **(b)**

**Figure 3.24:** $K$ along path for (a) relative template radius of 25% of the smallest dimension of the initial crack and (b) absolute template radius of 0.05 mm

### 3.4.5 Life evaluation in FRANC3D

To compute the number of cycles required to grow the crack front from one position to another, FRANC3D uses a "multiple variable degree of freedom" approach [16, p. 194]. First all nodes on front $i$ are projected perpendicularly from front $i$ onto the next crack front $i+1$ to find the intersection points. This is illustrated in Figure 3.25 where index $i$ represents the crack front, index $j$ is the node number on front $i$ and index $k$ is node numbers for crack front $i+1$. The SIF range $\Delta K$ is then found directly or interpolated at the intersection point on crack front $i+1$. A linear variation of $\Delta K$ is assumed between the two crack fronts, and the crack growth rate curve ($da/dN$-curve) is integrated to obtain the number of cycles. This is then repeated for all crack front nodes and an average is calculated to obtain the value of cycles required to grow from front $i$ to front $i+1$. This cycle counting procedure is illustrated more in detail in Figure 3.25.

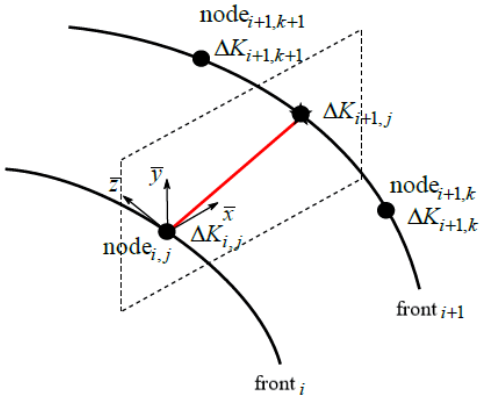


**Figure 3.25:** Computation of cycles along the crack front. Taken from [16]

### 3.4.6 Recommended settings for further analyses

Based on the studies in this chapter, the main recommended settings can be summarised as follows. These settings have also been used in further analyses in this thesis.

- Crack growth increment size: $\Delta a_{\mathrm{m}}$ should be larger than the template radius and approximately $0.2 \cdot \min(a, c)$

- Crack front fitting: Usually works fine with the default 3rd order fixed polynomial with 3% extrapolation. For long shallow cracks it's recommended to use a multiple polynomial. In some cases it's even necessary to increase the extrapolation and exclude some of the end points (located close to the free surface).

- Crack front mesh: Default settings, i.e. 3 rings and 8 circumferential elements,

are recommended. These settings might in some cases have an impact on the error "cannot triangulate new crack front surface" since it affects the overall crack front mesh.

- Template radius: Seen to affect the accuracy of the SIFs. Should be smaller than the crack growth increment and approximately $0.1 \cdot \min(a, c)$

## 3.5 Construction of FE-models

FRANC3D includes no possibilities to create FE-models starting from a CAD geometry file, so the base FE-models were created separately. The construction of FE-models were made to simulate the tests of Kb specimens in tension and bending, see section 2.4 for details about the test setup. First the FE-models were constructed in ANSYS to later be used in crack propagation simulations in FRANC3D. The forthcoming text will describe the modelling procedure in ANSYS.

The test specimens were modelled by use of ANSYS Mechanical APDL commands, and a *.cdb* file was created for the global uncracked model, it includes the global mesh, applied load and other boundary conditions. Elements used in the global model were SOLID186 20-node 3D quadratic elements with three degrees of freedom per node: translation in nodal $x$-, $y$- and $z$-directions [17].

The load and boundary conditions for tensile loading were applied according to Figure 3.26. The load was applied on the top-most surface as a pressure while the bottom surface was locked in $z$-direction. To allow for Poisson contraction, two lines were created at the bottom surface crossing the centre of the specimen - one parallel to the $x$-axis and one parallel to the $y$-axis. Nodes attached to these lines were then locked in $x$- and $y$-direction respectively to prevent rigid body motion.

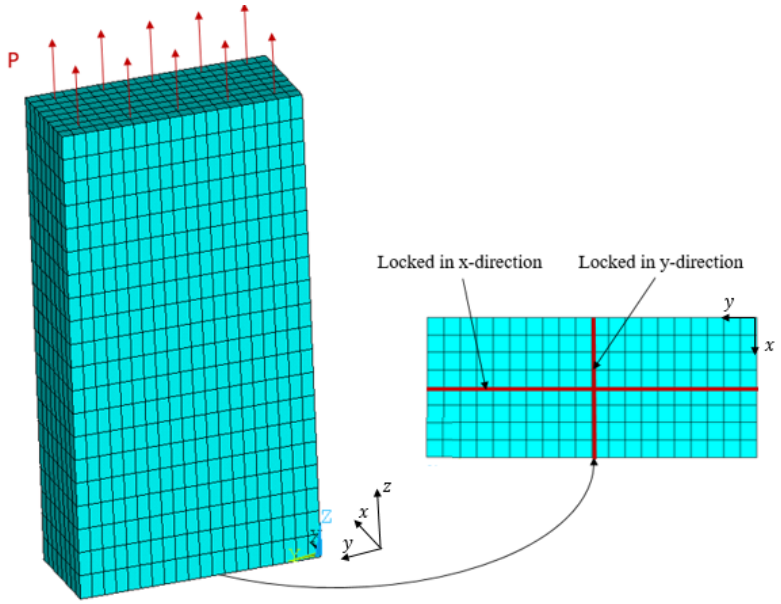


**Figure 3.26:** FE-model of Kb specimen for tensile loading. The model contains applied loads and boundary conditions

For four-point bending, loads and boundary conditions were applied according to Figure 3.27. The bottom edges at both ends were prevented to move in the $z$-direction, two nodes at one end-surface of the specimen were locked in $y$-direction while one node at the same surface was locked in $x$-direction to allow for Poisson contraction and not influence the stresses in the mid span of the specimen where crack growth occurs. The load was applied as line-loads parallel to the $x$-axis with an equal distance on both sides from the centre of the specimen.

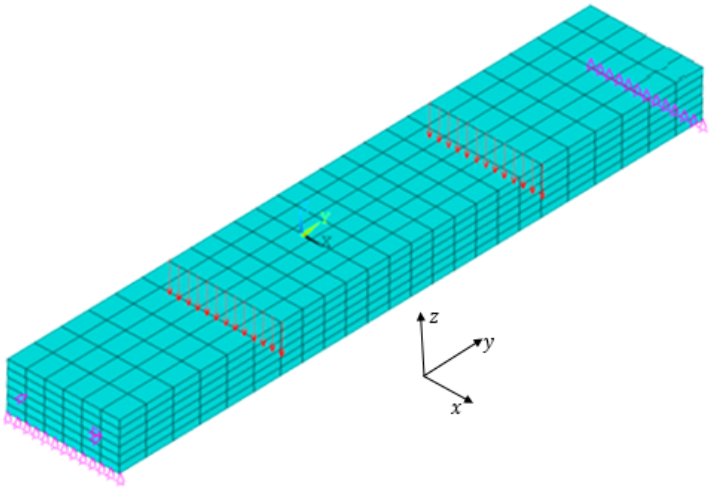


**Figure 3.27:** FE-model of Kb specimen for four-point bending loading. The model contains applied loads and boundary conditions

# 4

# Results

Two different test types were investigated by both FRANC3D and NASGRO: one tensile test and one four-point bending test, these consisted of 55 and 18 different test specimens respectively. The FE-models used for both test types are illustrated in section 3.5. The fracture mechanical attributes, i.e. number of cycles to final crack length and the corresponding crack shape were predicted by both programs and compared to test results. The quotient $N_{\text{test}}/N_{\text{pred.}}$ between the test and the predicted number of cycles was used in the comparisons.

The crack propagation testings were performed by GKN for different load magnitudes, load ratios, temperatures, initial crack sizes. The crack was propagated either until a target final crack size was reached or until final fracture. The settings used in FRANC3D were selected according to the recommendations in section 3.4.6.

The constants used in the crack propagation model and other relevant material data were provided by GKN for two different materials denoted Material A and B. Material A, a nickel-chromium-based alloy, was employed in both the tensile and bending cases, while Material B, a titanium-based alloy, was used for a cylindrical specimen with an embedded crack.

## 4.1 Tensile Loading

### 4.1.1 Test results

The tensile tests were performed at five different temperatures: 20, 400, 550, 600 and 650°C. The distribution of the 55 Kb specimens among the different temperature sets is seen in Table 4.1.

**Table 4.1:** Distribution of Kb specimens among the different temperature sets

| Temperature | 20°C | 400°C | 550°C | 600°C | 650°C |
|---|---|---|---|---|---|
| Number of tested specimens | 13 | 10 | 12 | 12 | 8 |

To illustrate the results, one test set performed at 550°C was chosen, since the trends for the different temperature sets were similar. The test parameters that were used for simulation are shown in Table 4.2. The corresponding numbers of test cycles seen in the last column are used for comparison to the predicted results from NASGRO and FRANC3D at the final crack length, $a_{\text{end}}$ in Table 4.2.

**Table 4.2:** Test results for test set at 550°C for tensile loading. ID number for the specimens, loading-, crack parameters and cycles to final crack length are shown from left to right

| Case ID | $\sigma_{\max}$[MPa] | $R$ | $a_{\text{start}}$ [mm] | $c_{\text{start}}$ [mm] | $a_{\text{end}}$ [mm] | $c_{\text{end}}$ [mm] | $N_{\text{test}}$ [-] |
|---|---|---|---|---|---|---|---|
| 24 | 649 | 0 | 0.565 | 0.583 | 2.33 | 2.35 | 9 011 |
| 25 | 648 | 0.5 | 0.565 | 0.578 | 2.34 | 2.43 | 23 020 |
| 26 | 647 | -1 | 0.635 | 0.600 | 2.20 | 2.40 | 4 696 |
| 27 | 624 | 0 | 0.498 | 0.529 | 2.23 | 2.15 | 10 421 |
| 28 | 624 | 0 | 1.10 | 1.12 | 2.52 | 2.48 | 2 833 |
| 39 | 750 | 0.5 | 0.517 | 0.564 | 1.67 | 1.61 | 6 441 |
| 30 | 626 | -1 | 0.610 | 0.579 | 1.83 | 1.92 | 2 679 |
| 31 | 750 | 0.5 | 1.15 | 1.12 | 2.39 | 2.53 | 6 623 |
| 32 | 624 | -1 | 0.619 | 0.659 | 2.22 | 2.46 | 2 129 |
| 33 | 624 | 0 | 0.786 | 0.723 | 2.36 | 2.48 | 4 646 |
| 34 | 750 | 0.5 | 0.686 | 0.716 | 2.35 | 2.39 | 8 365 |
| 35 | 625 | -1 | 0.565 | 0.645 | 1.82 | 2.01 | 2 649 |

### 4.1.2 Cycles to final crack length for test set at 550°C

Figure 4.1 shows the quotient $N_{\text{test}}/N_{\text{pred.}}$ for both NASGRO and FRANC3D. The case ID in Figure 4.1 corresponds to the parameters given in Table 4.2. A quotient equal to one means that the predicted number of cycles is the same as the actual number of cycles. NASGRO and FRANC3D were both overestimating and underestimating the number of cycles depending on the test case. NASGRO and FRANC3D were seen to predict similar results. The largest deviation between the two programs was seen for case ID 31 (9.1%), while the smallest deviation was seen for case ID 26 (2.6%).

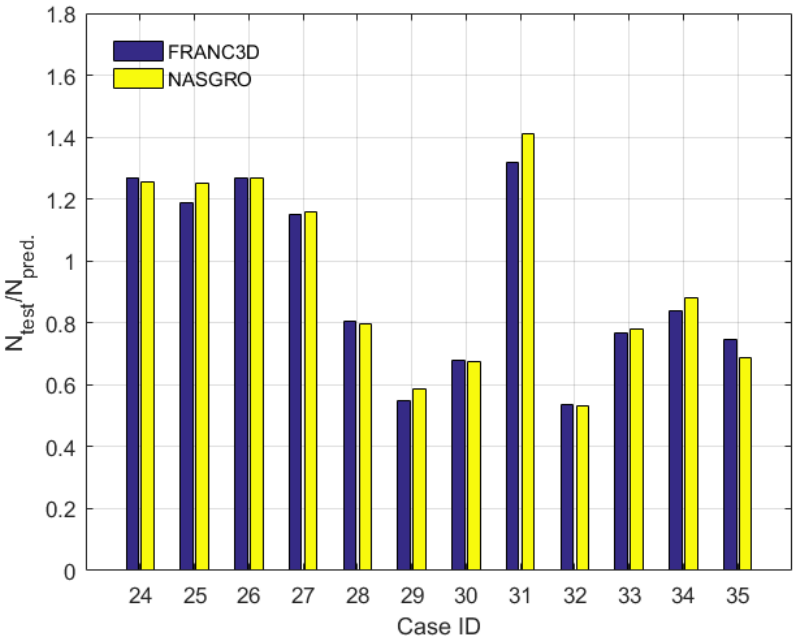


**Figure 4.1:** Comparison of $N_{\text{test}}/N_{\text{pred.}}$ between FRANC3D, NASGRO and test for tensile loading at 550°C

### 4.1.3 Crack shape at final crack length for test set at 550°C

The corresponding crack shape from NASGRO is characterised by the elliptical parameters $a$ and $c$, as described in section 3.2.1. The final crack length $a_{\text{end}}$ was set from test and the predicted final crack width $c$ was compared between the programs using the ratio defined in Equation (4.1), where the indices f and c means FRANC3D and NASGRO, respectively.

$$\chi = \frac{(c_{\text{f}} - c_{\text{c}})}{c_{\text{c}}} \tag{4.1}$$

FRANC3D always predicted a wider crack than NASGRO for the 550°C test set and a wider crack for the majority of the 55 Kb specimens. Figure 4.2 shows the crack shape between the largest and smallest deviation in $c$-direction seen for NASGRO and FRANC3D. These specimens have case IDs 27 and 35 respectively. The percentage difference, according to Equation (4.1), were 17.8 % and 5.6 % respectively. The graph in Figure 4.2 is defined by the values for $c$ and $a$ at the crack front, the curve is represented by a third degree polynomial fit between those points. The specimens that differed most in crack width did not correlate to the biggest percentage difference in life as discussed in section 4.1.2.

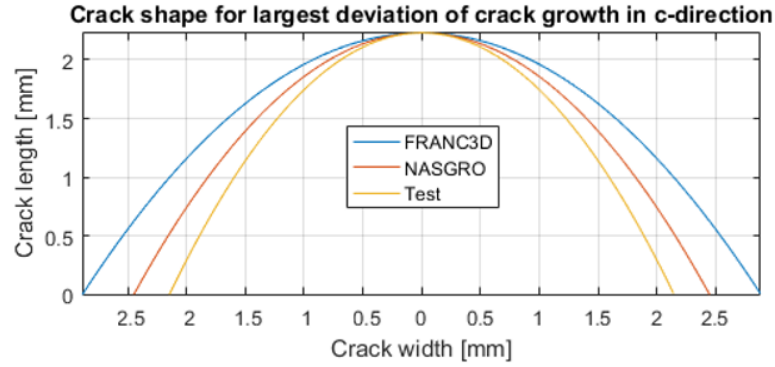


**(a)**

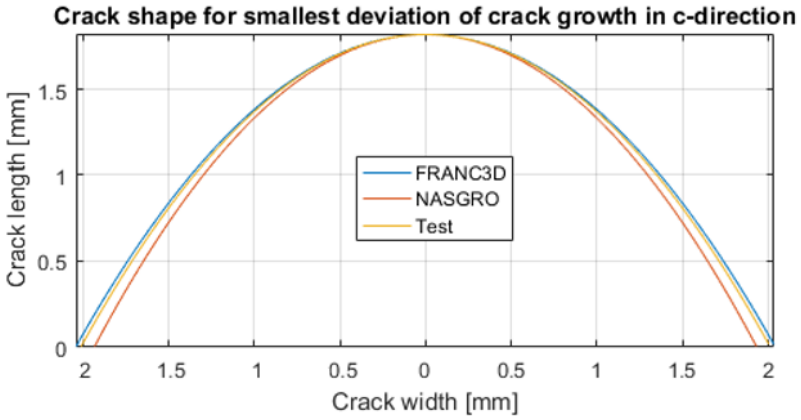


**(b)**

**Figure 4.2:** Comparison of crack shapes. (a) Largest and (b) smallest differences between FRANC3D and NASGRO

To investigate if there is a correlation between the crack shape and the SIF, the Mode 1 SIF was extracted from NASGRO and FRANC3D. The Mode 1 SIF was extracted for FRANC3D as described in section 3.1.4. The paths were chosen to capture $K$ at $a$ and $K$ at $c$, where the path for $K$ at $c$ in FRANC3D was chosen to be 5% of the total length of the crack front from the crack mouth since $K$ exactly at the free surface is unstable. The mode I SIFs are seen for case ID: 27 and 35 in Figure 4.3, where t in the legend stands for test case followed by case ID. NASGRO evaluates crack growth in $c$ with the calculated $K$ at $c$, which for crack growth includes the reduction factor described in section 3.2.1. This factor is accounted for in the results in Figure 4.3. FRANC3D is seen to have a higher SIF along $a$ and a smaller SIF along $c$ from about 3 mm up to the point were NASGRO stops propagating the crack. Between the test cases, the SIFs do not differ much, however the simulation in FRANC3D is seen to continue further for test case 27, i.e. the simulation is not intervened by numerical errors.

The SIFs from FRANC3D at the paths as specified above can be integrated in NASGRO. A one dimensional crack case in NASGRO was used for case ID 27. The

$K$ values for $a$ and $c$ were thus integrated independently of each other. The number of cycles was noted for $a_{\text{end}}$ and the corresponding growth in $c$ was evaluated at that number of cycles. The width became $c = 2.183\,\text{mm}$ which is a 10.8% more narrow crack than the standard NASGRO prediction, but closer to test data. This is anticipated since the SIF from FRANC3D was seen to be lower overall along $c$. FRANC3D predicts $c_{\text{end}} = 2.9470\,\text{mm}$ for the same SIF as used in NASGRO, this difference between the programs is attributed to the respective crack propagation method, i.e. crack front fitting, crack front propagation model and integration method.

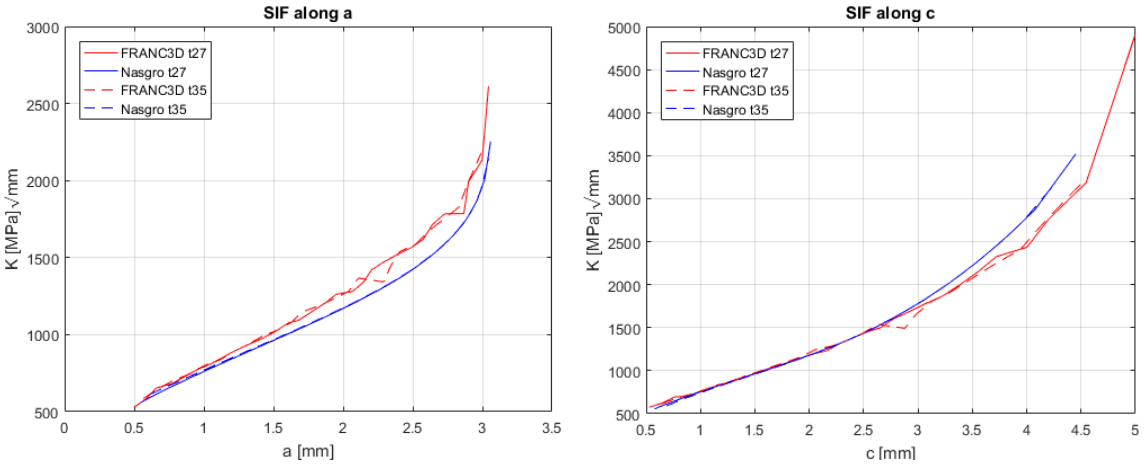


**(a)** **(b)**

**Figure 4.3:** SIF comparison between FRANC3D and NASGRO for test cases 27 and 35: (a) measured along $a$ and (b) measured along $c$ with an angle of three degrees from the free surface

#### 4.1.3.1 Effect of curve fit

The crack shape for test case 24 is seen in Figure 4.4. The crack from the test has a more oval shape as compared to the shape predicted by FRANC3D. The final crack width $c_{\text{end}}$ was 2.35 mm according to Table 4.2 whereas predicted width was 2.95 mm. This is a difference of 25%. Different curve fitting settings were investigated in section 3.4.2, where e.g. a moving polynomial was tested. Moving polynomial was seen to capture the behaviour of the crack at the free ends. The proposed curve fitting in FRANC3D for moving polynomial is different than the 3rd order polynomial as illustrated in Figure 4.5. The problems arising with this curve fitting make it not suitable for the automated simulations performed for the large number of specimens as considered in this thesis work.

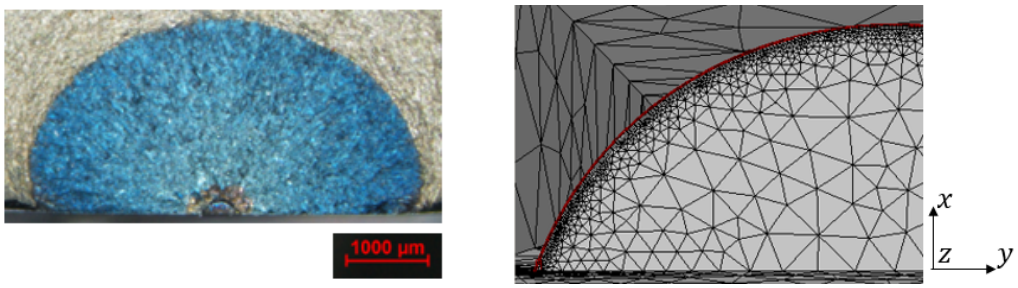


**(a)** **(b)**

**Figure 4.4:** Comparison of final crack shape between (a) test and (b) FRANC3D, for test case 24

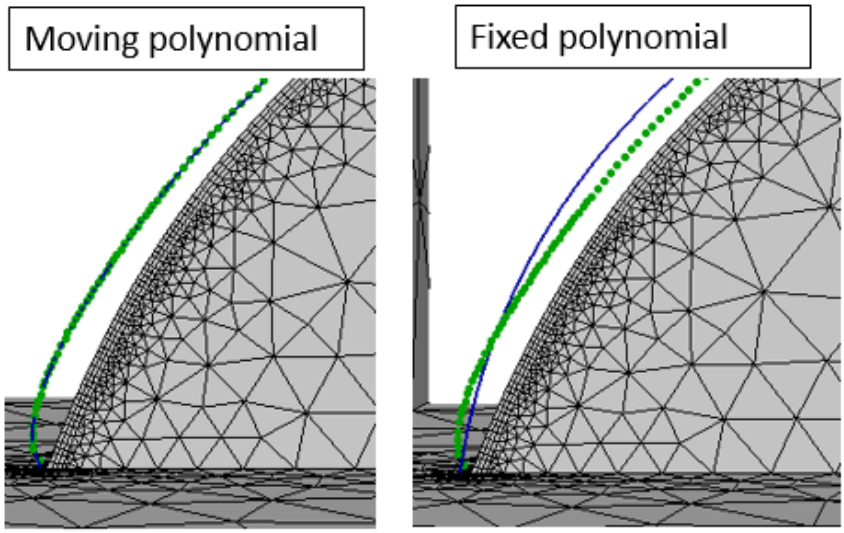


**Figure 4.5:** Comparison of curve fit for the crack front between moving polynomial and fixed polynomial

A change in settings was required when using moving polynomial, i.e. a smaller template radius and increment size. This increased simulation times. Changes in settings were also required after some crack growth steps to continue propagating the crack. An example of a successful simulation, which used a combination of both fixed and moving polynomial, was performed for test case 27. First using fixed polynomial with the recommended settings then a moving polynomial with smaller increment size and template radius. The corresponding crack growth in $c$- and $a$-directions versus number of cycles is seen in Figure 4.6, where indices 1 and 8 correspond to the moving and fixed polynomial respectively. The crack width at $a_{\text{end}}$ for the moving polynomial became 2.93 mm as compared to 2.89 mm for the fixed polynomial curve fit. Hence the crack growth is not much affected in this case. The crack was also predicted to grow faster for the moving polynomial, see Figure

4.6, where the difference in cycles between the two curve fitting methods became 1.61% at $a_{\text{end}}$.

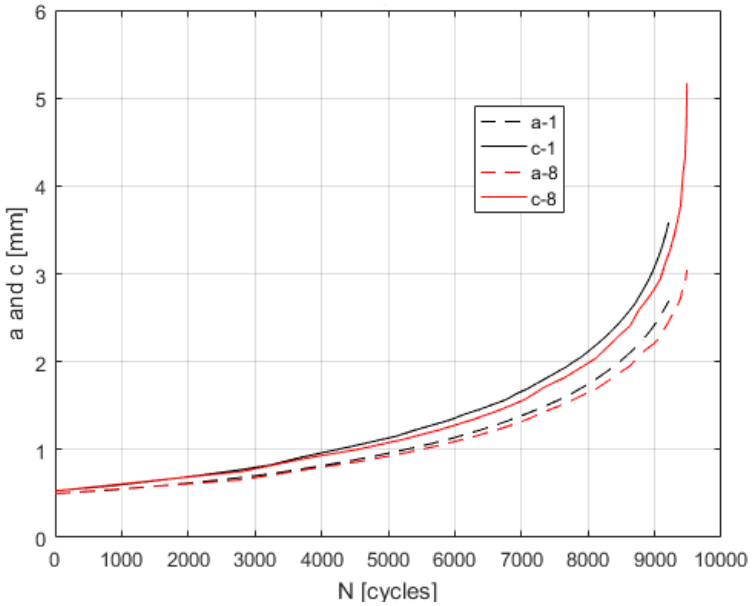


**Figure 4.6:** Crack growth for moving- and fixed-polynomial with indices 1 and 8 respectively (crack case 27)

## 4.2 Four-point Bending

### 4.2.1 Test results

All four-point bending tests were performed at room temperature. The $R$-ratio used was $R = 0$ and pre-cracks were generated under tensile fatigue at stress levels $\sigma_{\max} = 400\,\text{MPa}$ or $\sigma_{\max} = 500\,\text{MPa}$. The testing consisted of two test sets for crack propagation under bending fatigue. For test set 1, crack propagation was performed until target final crack sizes were reached (8 tests in total). For test set 2, crack propagation was performed until final failure (10 tests in total). All relevant test data is tabulated in Table 4.3 for both test sets.

**Table 4.3:** Four-point bending test data for both test set 1 and 2. The table includes the test case IDs, applied stress levels, initial crack sizes and the resulting number of cycles. Final crack sizes are included for test set 1

| Case ID | $\sigma_{\max}$ [MPa] | $a_{\text{start}}$ [mm] | $\overline{c}_{\text{start}}$ [mm] | $a_{\text{end}}$ [mm] | $\overline{c}_{\text{end}}$ [mm] | $N_{\text{test}}$ [-] |
|---|---|---|---|---|---|---|
| **Test set 1** | | | | | | |
| 1 | 700 | 0.517 | 0.520 | 0.939 | 1.179 | 23 076 |
| 2 | 700 | 0.501 | 0.556 | 0.908 | 1.177 | 25 234 |
| 3 | 700 | 0.560 | 0.572 | 1.754 | 2.566 | 41 130 |
| 4 | 700 | 0.515 | 0.528 | 1.772 | 2.519 | 45 833 |
| 5 | 700 | 0.619 | 0.641 | 0.998 | 1.258 | 24 467 |
| 6 | 700 | 0.470 | 0.483 | 1.013 | 1.205 | 30 040 |
| 7 | 700 | 0.660 | 0.643 | 1.727 | 2.504 | 44 568 |
| 8 | 700 | 0.604 | 0.627 | 1.795 | 2.627 | 43 226 |
| **Test set 2** | | | | | | |
| 9 | 600 | 0.515 | 0.522 | - | - | 96 981 |
| 10 | 600 | 0.523 | 0.564 | - | - | 78 644 |
| 11 | 700 | 0.493 | 0.544 | - | - | 54 121 |
| 12 | 700 | 0.512 | 0.487 | - | - | 50 777 |
| 13 | 800 | 0.537 | 0.533 | - | - | 36 574 |
| 14 | 800 | 0.504 | 0.553 | - | - | 32 889 |
| 15 | 600 | 1.101 | 1.006 | - | - | 43 930 |
| 16 | 700 | 1.031 | 0.981 | - | - | 31 681 |
| 17 | 800 | 1.004 | 1.043 | - | - | 19 505 |
| 18 | 900 | 1.993 | 2.099 | - | - | 6 145 |

### 4.2.2 Comparison of cycles to final crack length

Figure 4.7 shows the quotient $N_{\text{test}}/N_{\text{pred.}}$, illustrated as blue and yellow bars for FRANC3D and NASGRO respectively. The analyses were performed according to test set 1. NASGRO was slightly closer to the test results for all test specimens as compared to FRANC3D, except of case ID 1, where they became almost exactly the same. All analyses resulted in shorter lives as compared to test results. The predicted life was therefore seen to be conservative.

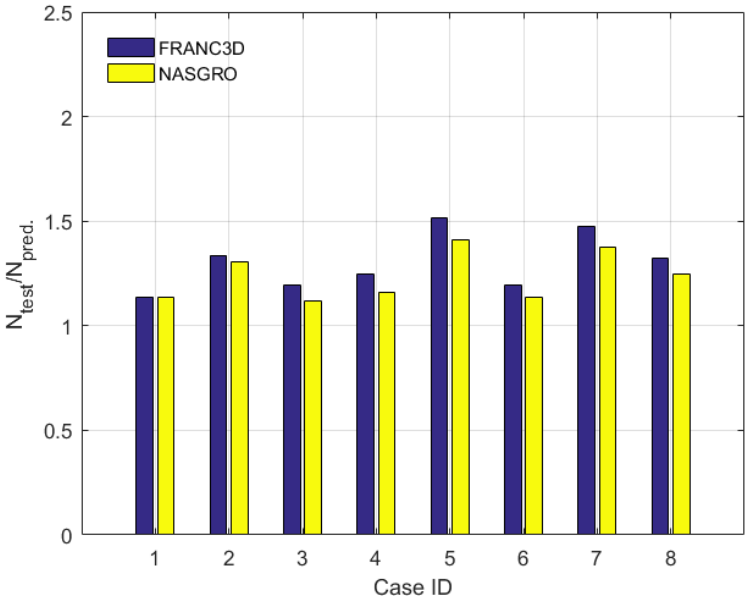


**Figure 4.7:** Test set 1, Four-point bending. Comparison of $N_{\text{test}}/N_{\text{pred.}}$ between FRANC3D, NASGRO and tests (cycles to target final crack sizes)

### 4.2.3 Comparison of cycles to failure

Figure 4.8 shows the quotient between the predicted number of cycles and the ones from testing, illustrated as blue and yellow bars for FRANC3D and NASGRO respectively. The analyses were performed according to test set 2. NASGRO is slightly closer to the test results for all test specimens as compared to FRANC3D. Predicted lives are conservative for all test cases.

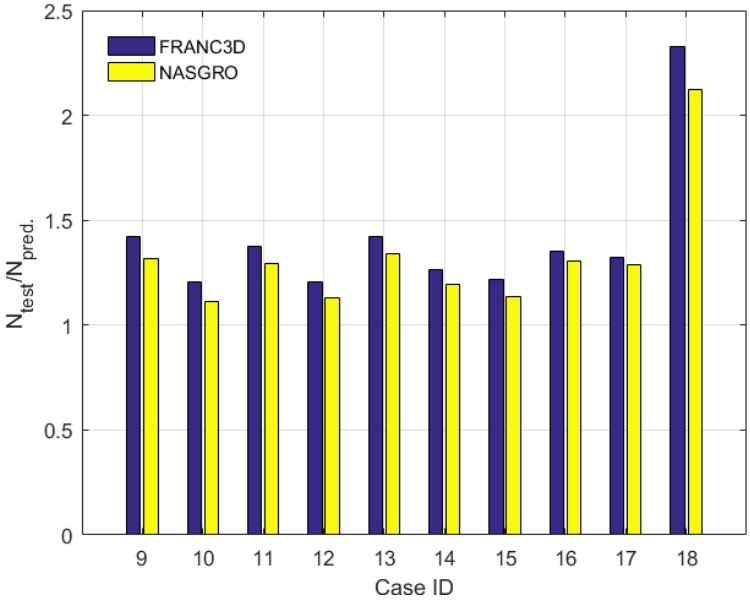


**Figure 4.8:** Test set 2, four-point bending. Comparison of $N_{\text{test}}/N_{\text{pred.}}$ between FRANC3D, NASGRO and test (cycles to failure)

## 4.3 Statistical evaluation

A large number of specimens were analysed for different loading, temperatures and initial and final crack sizes. It is customary to use a log-normal distribution for the comparison of the predicted and tested fatigue lives, since the error in prediction can be written as the logarithm of the ratio $N_{\text{test}}/N_{\text{pred.}}$ used in previous comparisons. An error, $e$, in prediction, according to [19], can be defined in the log-space as follows

$$\ln\left(N_{\text{test}}\right) - \ln\left(N_{\text{pred.}}\right) = e \tag{4.2}$$

and the expression can be re-written on the following form

$$\ln(N_{\text{test}}/N_{\text{pred.}}) = e. \tag{4.3}$$

Characteristics such as scatter in $e$ and how well the predictions match with test data on an average, i.e. how close the median (50%) value of $N_{\text{test}}/N_{\text{pred.}}$ is to 1, were used in the comparisons.

Figure 4.9 shows the log-normal probability plot for all tensile test cases. The quotient between the tested and predicted fatigue lives follows the log-normal distribution well, and a low scatter is observed for both predictions. The median values became 0.946 for FRANC3D and 0.954 for NASGRO. On average, the predictions matched well with test data as the median values were close to 1. Both methods are slightly over-predicting the fatigue life.

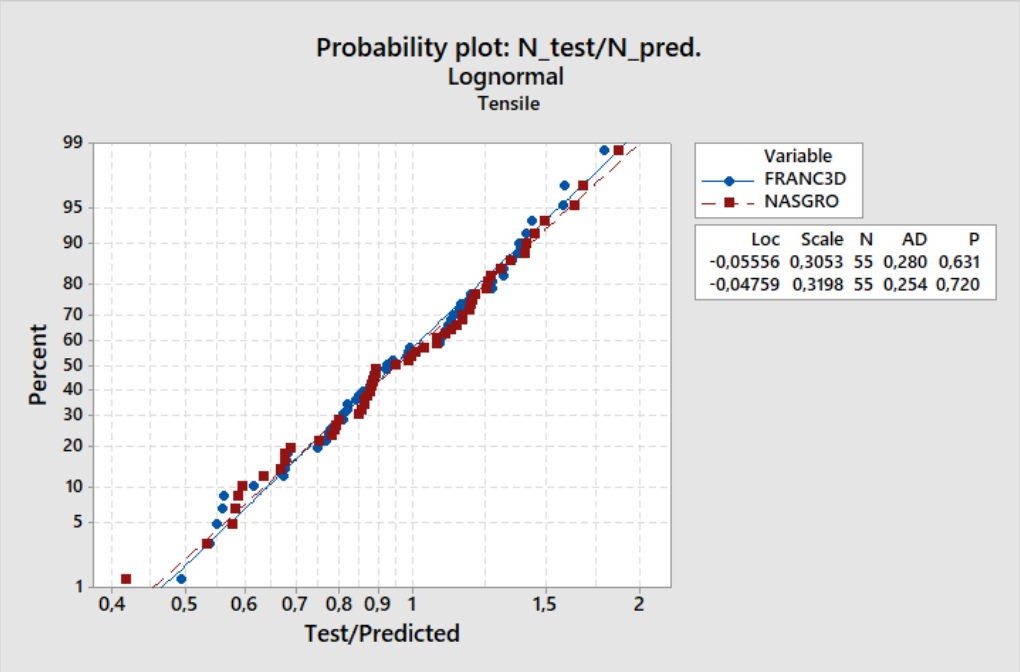


**Figure 4.9:** Log-normal probability plot for tensile test

The log-normal probability plots for test sets 1 and 2 for bending fatigue are shown in Figure 4.10a and 4.10b respectively. For test set 1, the median (50%) values

for FRANC3D and NASGRO were 1.297 and 1.232 respectively. Both FRANC3D and NASGRO have similar results, but NASGRO is slightly more conservative than FRANC3D for test set 1. For test set 2 more scatter was observed and the data points are not following the log normal distribution as good as for test set 1. For one test case, the two right most data points in Figure 4.10b, a large underestimation of the predicted fatigue life is observed for both FRANC3D and NASGRO. This has a large influence on the median value, since the data set is small. The median values for FRANC3D and NASGRO respectively became 1.385 and 1.301. The reason for the occurrence of these outlier data points is unknown.

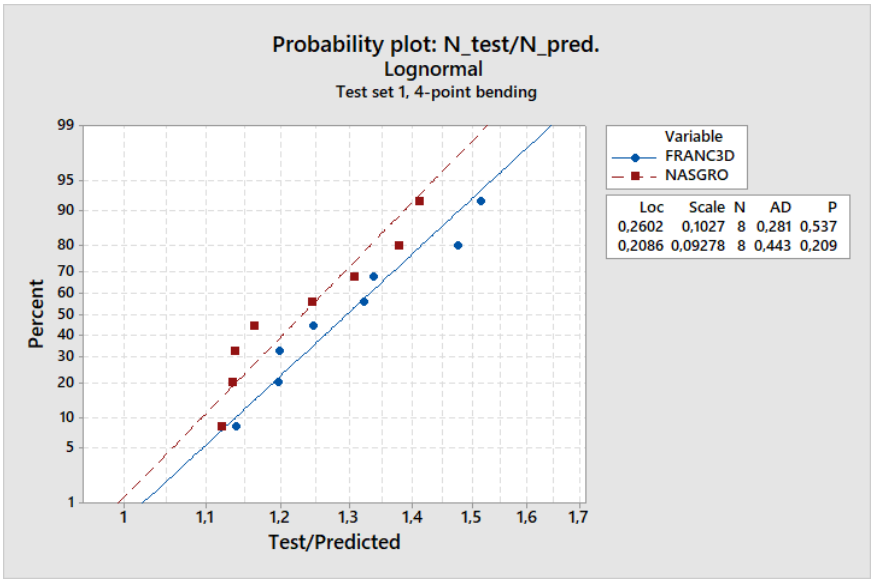


**(a)**

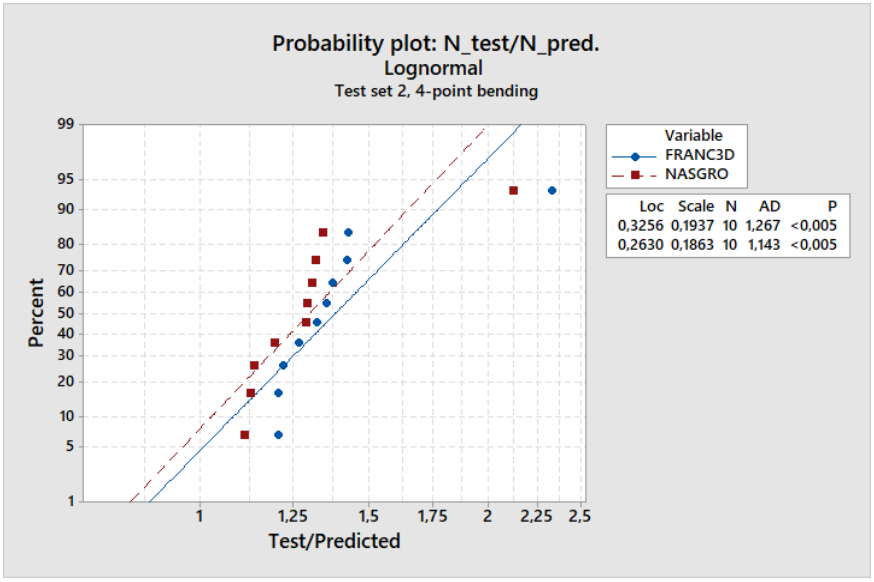


**(b)**

**Figure 4.10:** Log-normal probability plots for four-point bending (a) test set 1—cycles to final crack sizes and (b) test set 2—cycles to failure

## 4.4 Embedded crack in circular specimen

Test specimens with rectangular cross sections are used for fatigue testing by GKN. Another commonly used configuration in fatigue testing, e.g. according to ASTM E466, is a circular test specimen. It is of interest to see how well FRANC3D predicts the fatigue life in this case, as it allows for a more accurate modelling of the geometry of the specimen and crack shape. A circular specimen, with a crack type where handbook-type solutions were not available in NASGRO, was therefore considered. This configuration was defined as a cylindrical specimen with an embedded circular crack according to Figure 4.11. The analysis was carried out for tensile fatigue and Material B. Other relevant information, such as specimen dimensions, location of the embedded crack, load and boundary conditions are seen in Figure 4.11.

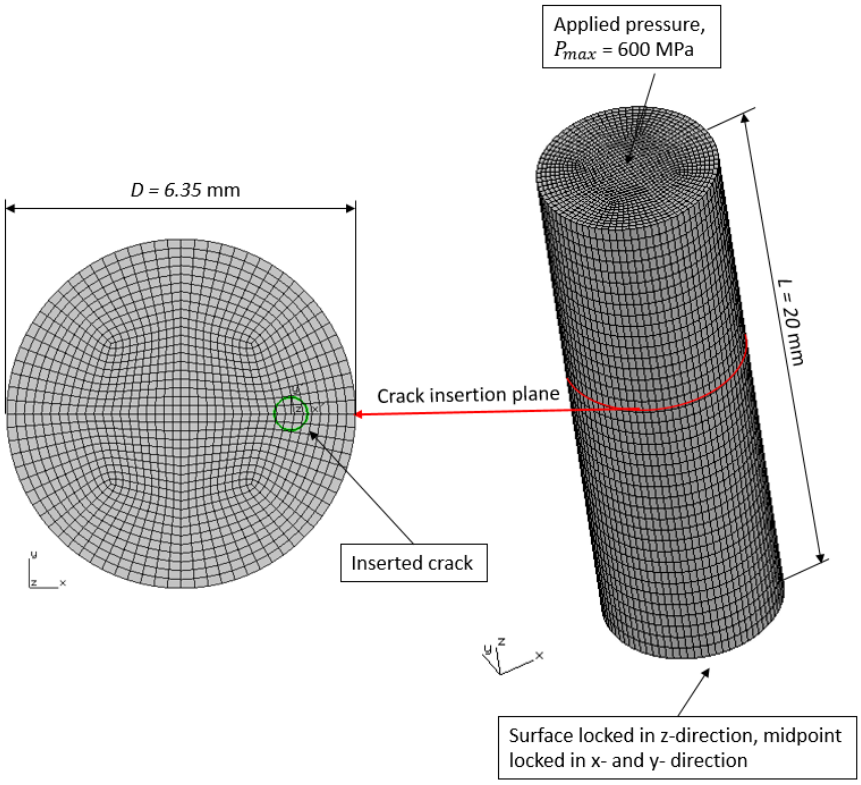


**Figure 4.11:** Initial mesh, load, boundary conditions and location of embedded crack in a cylindrical specimen modelled in FRANC3D

For comparison two similar crack types were selected in NASGRO, the crack types EC04 and SC07, EC04 features a square plate with an embedded crack and SC07 a cylinder with a surface crack as shown in Figure 4.12. For the analyses, the diameter of the embedded crack was set to a constant value $d = 0.4\,\text{mm}$ while the distance between the crack front and the outer free surface of the specimen varied from $l = 0.1\,\text{mm}$ to $l = 1.5\,\text{mm}$, see Figure 4.12. Note that SC07 is a surface crack, so the crack length was assumed to be the diameter of the embedded crack plus the distance from the free surface $a = d + l$.

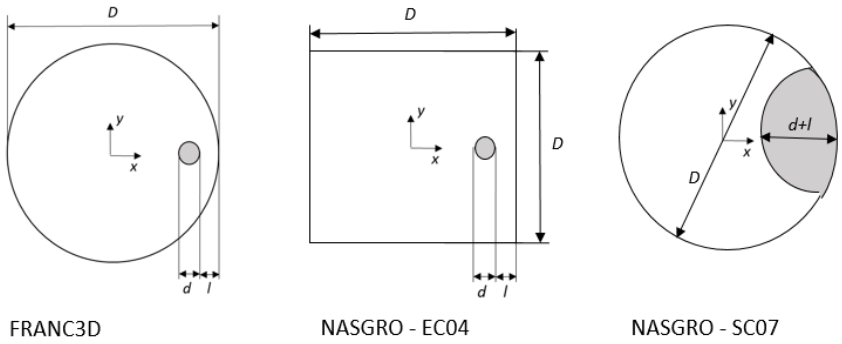


**Figure 4.12:** Initial crack size and location in FRANC3D and two crack types in NASGRO

The predicted number of cycles to failure and transition for the different crack sizes are presented in Table 4.4. It was also of interest to investigate when the embedded crack was predicted to transition to a surface crack. This was also included in the comparison. In Table 4.4 $N$ is the total number of cycles from the initial crack to failure and $N_{\text{tran.}}$ the number of cycles from the initial crack until the transition to a surface crack.

Employing SC07 resulted in conservative predictions with predicted fatigue lives significantly shorter than for FRANC3D and EC04. Both FRANC3D and EC04 resulted in approximately the same number of cycles until failure and transition. Initially an embedded crack close to the surface was assumed to be the most critical case. That seems to be true, if one only considers the total life. One interesting thing is that the portion of cycles after the crack has transitioned to a surface crack is very small as compared to the total life for larger $l$. This type of crack can be difficult to detect during inspection as it grows inside the specimen almost the whole life. Hence it might be more critical than the embedded crack located close to the surface, which grows as a surface crack for a larger portion of the total life.

**Table 4.4:** Predicted total life and cycles to transition for FRANC3D and NASGRO

| Distance | FRANC3D | | EC04 | | SC07 |
|---|---|---|---|---|---|
| from surface | $N$ | $N_{\text{tran.}}$ | $N$ | $N_{\text{tran.}}$ | $N$ |
| $l = 0.1\,\text{mm}$ | 12 136 | 5 900 | 12 000 | 4 298 | 4 331 |
| $l = 0.4\,\text{mm}$ | 15 537 | 13 300 | 15 625 | 12 774 | 1 696 |
| $l = 0.8\,\text{mm}$ | 18 066 | 17 200 | 17 704 | 16 810 | 516 |
| $l = 1.5\,\text{mm}$ | 19 913 | 18 886 | 19 432 | 19 362 | 34 |

# 5

# Conclusions

Fatigue crack propagation in titanium and nickel based alloys has been studied for two different types of loading. The main purpose has been to evaluate the crack propagation tool FRANC3D in comparison to handbook-type solutions and tests. To this end, the crack propagation of a surface crack in a Kb test specimen has been evaluated through numerical analyses and handbook-type solutions. A study of different settings in FRANC3D has been performed and a list of recommended settings has been presented. Analyses have been validated against available test data. Crack propagation predictions have also been performed for an embedded crack in a circular specimen for which handbook-type solutions were not available.

Based on these investigations the following can be concluded:

- Appropriate settings for crack propagation analysis in FRANC3D have been proposed and shown to give stable results for the simulated test specimens.
- It has been shown that FRANC3D, where the crack is explicitly modelled in FEM, gave similar number of cycles as a more traditional handbook-type solution approach, such as NASGRO. This was the case both for propagation to a specified crack length and to final failure. Both programs were shown to have a statistical mean life prediction that was close to the mean life prediction of the 55 Kb specimens in the tensile tests. The programs gave similar predictions for the bending case but in addition to the tensile tests, the predictions were conservative. That is, they predict a shorter mean life than the mean life from tests.
- FRANC3D has been shown to have more freedom to capture the crack shape than NASGRO through different types of curve fitting to approximate the crack front.
- FRANC3D predicts a wider crack, than NASGRO and test results, for the majority of the tensile tested Kb specimens.
- FRANC3D has been shown to be sensitive to user settings, i.e the program demands more effort from the user than what is required for running cases already defined in NASGRO.

- FRANC3D was shown to be able to perform crack growth simulation for an embedded crack in a circular specimen, where a corresponding NASGRO crack type is not available.

## 5.1 Recommendation for future work

It has been shown that FRANC3D has capabilities to simulate crack growth in configurations such as embedded cracks in a circular specimens. Aero-engine components, such as struts used for guiding hot air and carry the weight of the engine, are of interest to analyse for fatigue. Components like this are subjected to heat which may vary with fatigue cycles. They also have more complex geometries which might be possible to analyse in FRANC3D.

FRANC3D also includes possibilities to perform fatigue analysis for mixed mode loading, where the crack can propagate in directions outside of the crack plane. There are several settings available in order to specify the direction of crack propagation. It would be of interest to investigate these setting more in detail.

Some aspects to investigate further could thus be:

- Investigate the capabilities of simulating thermal fatigue in FRANC3D, i.e; temperature variation in space and time (cycles). Perform validation studies for these tests.
- Perform fatigue analysis on aero-engine components and validate—if possible, against test data.
- Perform crack propagation analysis for mixed mode loading.

# References


[1] L. Zhu, N. Li and P. R. N Childs, "Lightweighting in Aerospace Component and System Design", *Tech Briefs Magazine*, March, 2019. [Online]. Available: `https://www.techbriefs.com/component/content/article/tb/features/articles/33914`, Accessed on: May 05, 2020.

[2] Southwest Research Institute, "NASGRO® Fracture Mechanics & Fatigue Crack Growth Software". [Online]. Available: `https://www.swri.org/consortia/nasgro`, Accessed on: Jan. 24, 2020.

[3] T. L. Anderson, *Fracture Mechanics: Fundamentals and Applications*, 2nd ed., Boca Raton, FL, USA: CRC Press, 1995.

[4] Wikimedia Commons, "File: Fracture modes v2.svg", 2014. [Electronic image]. Available: `https://commons.wikimedia.org/w/index.php?title=File:Fracture_modes_v2.svg&oldid=142763665`, Accessed on: May 04, 2020.

[5] N. E. Dowling, *Mechanical Behaviour of Materials: Engineering Methods for Deformation, Fracture, and Fatigue*, 4th ed., London, UK: Pearson Education, 2012.

[6] B. Broberg et. al., *Handbok och formelsamling i Hållfasthetslära*, 11th ed., Stockholm, SWEDEN: Instant Book AB, 2014.

[7] L. Banks-Sills and D. Sherman, "Comparison of methods for calculating stress intensity factors with quarter-point elements", *Int. Journal of Fracture*, vol. 32, pp. 127-140, 1986.

[8] *NASGRO 9.1 Manual*, Southwest Research Institute, San Antonio, TX, USA, 2019.

[9] J. F. Yau, S. S. Wang and H. T. Corten, "A Mixed-Mode Crack Analysis of Isotropic Solids Using Conservation Laws of Elasticity", *Journal of Applied Mechanics*, vol. 47, pp. 405-421, June 1980.

[10] P. Wawrzynek, B. Carter and L. Banks-Sills, "The M-Integral for computing

stress intensity factors in generally anisotropic materials", National Aeronautics and Space Administration, Marshall Space Flight Center, 2005.

[11] M. Nejati, A. Paluszny and R. W. Zimmerman, "A disk-shaped domain integral method for the computation of stress intensity factors using tetrahedral meshes Integral", *Int. Journal of Solids and Structures*, vol. 69-70, pp. 230-251, 2015.

[12] J. R. Rice, "A Path Independent Integral and the Approximate Analysis of Strain Concentrations by Notches and Cracks", *Journal of Applied Mechanics*, vol. 35, pp. 379-386, 1968.

[13] N. S. Ottosen and H. Petterson., *Introduction to the FINITE ELEMENT METHOD*, Lund, SWEDEN: Prentice Hall, 1992.

[14] R. O. Ritchie, "Influence of Microstructure on Near-Threshold Fatigue-Crack propagation in Ultra-High strength steel", *Metal Science Journal*, vol. 11, no. 8-9, pp. 368-381, Sep. 1977, doi:10.1179/msc.1977.11.8-9.368.

[15] P. Wawrzynek, B. Carter and A. Ingraffea, "Advances in simulation of arbitrary 3D crack growth using FRANC3D/NG", *Journal of the Computational Structural Engineering Institute of Korea*, vol. 23, Jan. 2010.

[16] *FRANC3D Reference Manual*, Fracture Analysis Consultants, Inc., Ithaca, NY, USA, Version 7.4, 2019.

[17] *Verification Manual: Mechanical APDL*, ANSYS Inc., Canonsburg, PA, USA, version 18.1, 2014.

[18] *FRANC3D Benchmark Examples*, Fracture Analysis Consultants, Inc., Ithaca, NY, USA, Version 7.4, 2019.

[19] S. Roychowdhury, T. Månsson and T. Hansson, "Failure Assessment of Test Coupons: Comparison Between Model Predictions and Test Results", *Proceedings of the ASME Turbo Expo 2018: Turbomachinery Technical Conference and Exposition*, June 2018, doi:10.1115/GT2018-75734.

**DEPARTMENT OF MECHANICS AND**
**MARITIME SCIENCES**
**CHALMERS UNIVERSITY OF TECHNOLOGY**
Gothenburg, Sweden
www.chalmers.se


CHALMERS
UNIVERSITY OF TECHNOLOGY